Thesis for the degree of licentiate of Engineering

Ultra-sensitive measurements of magnetically labelled RCA products in a microfluidic channel using a high-T_c SQUID

Sobhan Sepehri

CHALMERS
UNIVERSITY OF TECHNOLOGY

Department of Microtechnology and Nanoscience
Quantum Device Physics Laboratory
Chalmers University of Technology
Göteborg, Sweden 2018

Ultra-sensitive measurements of magnetically labelled RCA products in a microfluidic channel using a high-T_c SQUID
SOBHAN SEPEHRI

Techinical Report MC2-384
ISSN 1652-0769

Chalmers University of Technology
Department of Microtechnology and Nanoscience- MC2
Quantum Device Physics Laboratory
SE-412 96 Göteborg, Sweden
Telephone +46 31 772 1000

Printed by Reproservice
Göteborg, Sweden 2018

Ultra-sensitive measurements of magnetically labelled RCA products in a microfluidic channel using a high-T_c SQUID

SOBHAN SEPEHRI
Department Microtechnology and Nanoscience
Chalmers University of Technology

Abstract

The development of a nucleic acid (deoxyribonucleic acid (DNA), ribonucleic acid (RNA)) bioassay based on magnetic nanoparticles (MNPs) with a high-T_c superconducting quantum interference device (SQUID) gradiometer as a magnetic readout is described. The specific binding of the MNPs to the target DNA molecules changes the MNPs size distribution and, therefore, the relaxation dynamics and is measured by magnetic ac susceptometry. The binding reactions are measured by SQUID gradiometer in a microfluidic channel with volume of 3 µL. The magnetic content sensitivity at the noise level of our SQUID is estimated to be 1.5×10^6 MNPs/$\sqrt{Hz}$ or 2.9×10^{-10} $emu/\sqrt{Hz}$ in magnetic moment, corresponding to 2.5 ng of MNPs with diameter of 100 nm.

Two different assay protocols are investigated for a magnetic nucleic acid biosensor. Padlock probes with suitable sequences are used as bioreceptors and circularize upon target recognition. The rolling circle amplification (RCA) provides the gain to the target molecule by copying the circularized padlock probe into a large concatemer. The specific binding of the MNPs to these large DNA coils changes their relaxation dynamics. These large DNA molecules can also digest into short monomers. The monomers can induce an agglutination if two MNP with matching sequence motifs to the two ends of the monomer are introduced. The agglutinated clusters would have large hydrodynamic size, thus, a different relaxation dynamics. The bioassay has shown higher sensitivity using large DNA coils. Extrapolated sensitivity of the sensor to target analyte is estimated to be 66 fM of RCA coils. This is limit is equivalent to 1.0×10^5 target DNA molecules.

The method and instruments that are adopted and presented here are not limited to the *Vibrio cholera* bioanalyte and are generic and could in principle be used for other DNA or RNA viruses. The ultra-high magnetic sensitivity combined with the microfluidic sample handling is a critical step towards a magnetic bioassay for rapid detection of diseases at the point-of-care (POC). Future developments include implementation of all steps of the bioassay on a disposable lab-on-chip and eliminating the liquid nitrogen by operating the SQUID on a micro-cooler platform. These would make the magnetic bioassay promising for applications as a future nano-diagnostics unit.

Keywords: magnetic bioassay, biosensor, high-T_c SQUID, rolling circle amplification, magnetic nanoparticle, diagnostics.

Acknowledgements

I would like to first and formost thank my supervisor Alexei Kalaboukhov for his time, support, and valuable guidance. I want to extend this gratitude to my co-supervisor Justin F. Schneiderman and examiner Dag Winkler for their assistance and feedback. I am honored to have you on my side.
This work would have not been possible without the collaborations with Teresa Zardán Gómez de la Torre, Christer Johansson, Jakob Blomgren, Maria Strømme, Aldo Jesorka, Kiryl Kustanovich, Jan Albert, Mats Nilsson, Ivan Hernandez-Neuta and Felix Neumann. Teresa made valuable contribution with her samples from Uppsala. Aldo and Maria opened their labs to me. Discussions with Christer and his passion for magnetism have been inspirational. I look forward to continuing collaboration with all of you.
Lars Jönsson you never fail to surprise me with your skillful craftsmanship. You are a true asset to the quantum device physics laboratory (QDP). Susannah Carlsson and Maria Tremblay, I appreciate all your administrative support.
Silvia Ruffieux, Christoph Pfeiffer, Minshu Xie and Maxim Chukharkin Leonidovich thank you for all your help in the SQUID lab in particularly for reading the numbers on the lock-in. You are great colleagues and friends. Silvia thank you for carefully reading this thesis hunting all my missed/misplaced articles. I hope you do not find any in the acknowledgment. Special thanks also to all members of QDP, applied quantum physics (AQP) and newly formed quantum technology (QT) laboratories including friends and colleagues: Riccardo, Eric, Gunta, Nastaran, Fatemeh, Giovanni, Angelo, and my old and new gym buddies Edoardo and Marco. You have created an amazing stimulating environment.
Last, but not least, I wish to thank my friends and family. Especially my parents, Hamid and Mina, for their love, support and patience.

Sobhan Sepehri, Göteborg, January 2018

List of publication

This thesis is based on the work contained in the following paper:

S. Sepehri et al. “Volume-amplified magnetic bioassay integrated with microfluidic sample handling and high-Tc SQUID magnetic readout”. *APL Bioengineering* 2.1 (Mar. 2018), p. 016102

Other papers and publications:

A. Kalabukhov et al. “Operation of a high-Tc SQUID gradiometer with a two-stage MEMS-based Joule Thomson micro-cooler”. *Supercond. Sci. Technol.* 29.9 (2016), p. 095014

F. Ahrentorp et al. “Sensitive magnetic biodetection using magnetic multi-core nanoparticles and RCA coils”. *J. Magn. Magn. Mater.* (2016), pp. 14–18

Contents

1

Aim and outline

In this thesis, we describe the development of a sensitive magnetic nucleic acid bioassay based on magnetic nanoparticle (MNP) labels using high-T_c superconducting quantum interference device (SQUID) gradiometer readout and microfluidic sample handling. Padlock probe ligation is exploited for target recognition followed by an amplification method, rolling circle amplification (RCA). The detection of the target is based on the immobilization of MNP labels on RCA products and is measured using magnetic ac susceptibility. The development is a part of the FLU-ID project supported by the Swedish Foundation for Strategic Research, SSF. The ultimate goal of the project is development of a portable nano-diagnostics unit for detection of pandemic influenza. The unit should have high specificity and sensitivity, low cost, and fast response.

The thesis is divided into three main parts: the first chapter describes the details of different elements of nucleic acid assay, namely the target recognition, amplification and the specific binding to biomarkers and the relaxation processes associated with MNPs which are used for detection of the target analyte. The second chapter gives a short introduction into the principles of operation of the SQUID and presents the SQUID gradiometer sensor developed for this project. In order to have better control over the volume and geometry of the samples, microfluidic channels are used. The basics and fabrication of the microfluidic chip is explained. The experimental ac susceptibility setup is then described following a model that simulates the flux from the ferrofluidic samples inside the microfluidic chips coupling to the pick-up loops of the SQUID gradiometer. Chapter 4 covers the measurements of MNPs and the RCA products both in form of large RCA coils and short digested monomers. Chapter 5 summarizes the performance and sensitivity of the assay and the detection method and gives an outlook on future work towards a point-of-care (POC) nano-diagnostic unit.

2

Biomagnetic assay

Biosensors are analytical devices utilizing the high sensitivity and selectivity of biological sensing. They are comprised of two main components: (I) a bioreceptor and (II) signal transduction. Bioreceptors are biological recognition elements that discriminate and distinguish the target analyte, e.g. antigen/antibody, deoxyribonucleic acid (DNA), cell, etc. The biorecongnition is not necessarily measurable and therefore, a signal transduction is necessary. Signal transduction is a process which translates the biological signal into a measurable physical signal. Numerous signal transduction methods are used in biosensors: fluorescence [4], electrochemistry [5], Raman scattering [6], field effect transistors [7], magnetoresistance [8], planar hall sensors [9], magnetic susceptibility [10] just to name a few. There is a diverse variety of biosensors combining different biological recognition elements with different signal transduction methods.

Nucleic acid assays are a group of biosensors that adopt DNA as bioreceptor. They use a single-strand DNA which hybridizes to its complementary strand with good specificity to realize the detection of a specific DNA or ribonucleic acid (RNA) target. These nucleic acid-based sensors can be used to detect pathogens, infection diseases etc. Functionalized nucleic acids like aptamers and DNA enzymes have broadened the applications to detect inorganic and organic molecules and even organisms [11]. The nucleic acid assays are simple and accurate due to the DNA hybridization technique and therefore, have attracted a lot of attention leading to new developments and technologies. The sensitivity of these biosensors depends mainly on three factors: the efficiency of the sequence hybridization, the sequence amplification method, and sensor sensitivity. The hybridization efficiency is affected by the structure of the probe and target, the hybridization condition and molecular interactions, etc. [12]. The sequence amplification is a necessary step to reach sensitivities that are required in diagnostic laboratories. There are several amplification methods available, such as polymerase chain reaction (PCR) [13], loop mediated isothermal amplification (LAMP)[14], ligase chain reaction (LCR)[15], and RCA[16]. Many of the above mentioned signal transduction methods, e.g. fluorescence, electrochemistry, etc., among others are currently used in the nucleic acid assays. However, sensitive signal transduction is still one of the bottlenecks biosensors face in practical applications.

Recent developments in nanotechnology have allowed the use of nanostructures such as nanoparticles, nanotubes, nanowires, etc. in biosensors. MNPs have a wide range of applications in biology and medicine [17, 18, 19]. The developments in the synthesis and coatings of MNPs [20] have given them a biological recognition function. MNPs are now used as labels for detection, mobile substrates for binding to target analyte or both as substrate and label at the same time [21]. Bioassays based on MNPs have the advantage of real-time detection and low level of background signal. They also do not require immobilization or intermediate washing steps making them advantageous for biosensing [22].

2.1 Nucleic acid assay

The genetic information encoded as a sequence of monomers in nucleic acids, DNA and RNA, are responsible for cellular function and consequently essential for all forms of life. The building block monomers are nucleotides which are made of a 5-carbon sugar, a phosphate group and a nitrogenous base. Nucleic acid diagnostics measure DNA or RNA in order to assay a particular nucleic acid sequence. To detect low abundant nucleic acids, numerous methods have been developed which selectively copy a specific and pre-defined nucleic acid sequence [23, 24].

The first and most commonly used nucleic acid amplification method is PCR. It is simple, easy, and has been broadly validated. The PCR technique relies on thermal cycling of the reaction for replication and amplifies a specific target DNA sequence to large number of copies. Despite all its advantages, PCR has its limitations, such as chances of contamination, sensitivity to certain contaminants, inhibitors, and thermal cycling [25].

There are several alternative amplification methods to PCR that offer potential advantages for speed, scale, cost and simplicity, e.g. LAMP[14], LCR[15], and RCA[16]. In our bioassay we are using the RCA technique for amplification. RCA is an isothermal amplification and enables enzymatic amplification of the probe-target complex. The biomolecular detection technique utilizes a highly specific hybridization reaction between a probe molecule and a matching target forming a probe-target complex. This proves to be advantageous for genotyping or mutation detection in a unrelated background. The probe-target complex can then be amplified in order to achieve high sensitivity in single-molecule detection [25, 26].

The probes are synthetic linear oligonucleotides containing target complimentary regions at the ends. Upon conjugation with matching DNA target, the two ends of the probe are brought together forming a circularized padlock probe. Probes are then closed by ligation. The ligation is sensitive to any mismatch at the $3'$ end of the probe molecule. The circular probes are extended by continuous progression of $\Phi 29$ DNA polymerase around the padlocks turning them into long single stranded concatemer DNA molecules. These large DNA molecules (also called DNA coils)

contain complementary sequences of the circular probe-target complex, Fig. 2.1. Throughout this work, synthetic *Vibrio cholera* target DNA is used. The DNA sequences used in this study for *Vibrio cholera* target, padlock probe and detection oligonucleotide are presented in Table 2.1. The procedure which has been used to produce final RCA products of 5 nM concentration is explained in the following sections.

Table 2.1: DNA sequences used in this study for synthetic target *Vibrio cholera*, the padlock probe and the detection oligonucleotide.

Target *Vibrio cholera*	5′-CCC TGG GCT CAA CCT AGG AAT CGC ATT TG-3′
Padlock probe for *Vibrio cholera*	5′-TAG GTT GAG CCC AGG GAC TTC TAG AGT GTA CCG ACC TCA GTA GCC GTG ACT ATC GAC TTG TTG ATG TCA TGT GTC GCA CCA AAT GCG ATT CC-3′
Detection oligonucleotide	5′-Biotin-TTT TTT TTT TTT TTT TTT TTG TTG ATG TCA TGT GTC GCAC-3′-FAM

2.1.1 Padlock probe target recognition and ligation

The padlock probe is a synthesized linear oligonucleotide, typically consisting of 70-100 nucleotides in length [27]. Around 20 outermost nucleotides at both 3′ and 5′ ends of the padlock are sequences complementary to the target DNA sequence. Therefore, they hybridize to the target DNA sequence in juxtaposition. The rest of the sequence linking the two hybridization arms are used for detection and identification.
In order to form a probe-target complex, 3 µl synthesized target *Vibrio cholera* DNA (1 µM) was hybridized and ligated at 37 °C for 15 minutes with 1 µl padlock probe (1 µM) in a solution consisting of 2.5 µl of 20 mM adenosine triphosphate (ATP), 1 µl T4 DNA ligase (1U/µl, enzyme unit per micro liter), and 5 µl of Φ29 DNA polymerase buffer in a total volume of 50 µl. After the probes are conjugated to the targets, a ligase mediated process closes the snick in between the two ends and topologically locks the padlock to the target. The ligation process is very sensitive to any mismatch at the 3′ end of the padlock probe molecule. This allows an excellent sequence probing and detects any mutations down to single nucleotide [28, 29].

2.1.2 Amplification

The circularized padlocks are then amplified by continuous progression of Φ29 polymerase around the circular DNA padlock probe replicating its sequence. In order to amplify the padlock probes, 25 µl ligation mix consisting of 20 nM concentration of padlock probes are copied by 0.4 µl Φ29 polymerase for 1 hour at 37 °C in a solution with 4 µl nucleotide triphosphate (dNTP) (2.5 mM), 6 µl bovine serum albumin

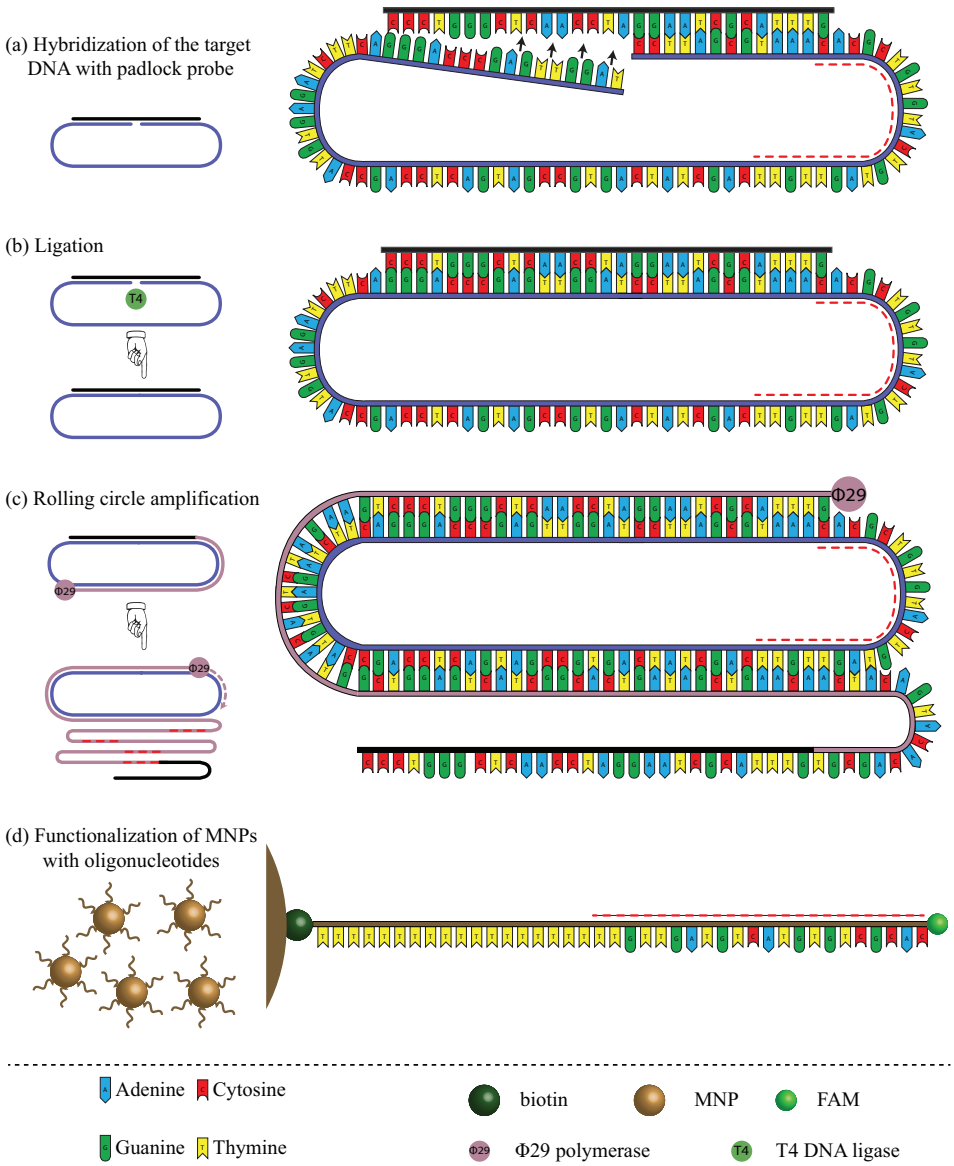

Figure 2.1: Illustration of (a) padlock probe recognition of synthetic *Vibrio cholera* target DNA , (b) ligation, (c) the amplification of the probes by RCA and (d) functionalized MNP for specific binding to the RCA coils. The oligonucleotide tags are bound to the streptavidin shell of the MNPs by a biotin molecule.

(BSA) (2 µg/ml), 6 µl Φ29 polymerase buffer and water in 60 µl reaction volume. The enzyme is thermally inactivated at $65°C$ for 5 minutes. A hybridization buffer of 1 M Tris(hydroxymethyl) aminomethane hydrochloride (Tris-HCl) (pH 8.0), 0.5 M ethylenediaminetetraacetic acid (EDTA), Tween-20(10%) and 5M sodium chloride (NaCl) was added at the end [30]. The one hour reaction produces approximately 1000 complimentary copies of the circularized probe-target complex, joining them end-to-end within a single DNA macromolecule [29].

2.1.3 Oligonucleotide tagged MNP probes

The RCA products need to be labeled before they can be detected. They are detected optically or magnetically by addition of fluorescent or magnetic labels, respectively. The labels have complementary oligonucleotides to linking part of the base sequence RCA products which allow them to hybridize with the DNA coils. This results in crowding the labels around the DNA coils which can be detected optically or magnetically. In this work streptavidin-coated MNPs are used as physical labels for detection. A biotin molecule is added to the detection oligonucleotide and the high affinity of streptavidin for biotin binds the oligonucleotides to the MNPs. On the other end of the detection oligonucleotide there is also a fluorescent label which allows optical detection of the DNA coils, Fig. 2.1.

The coupling of the oligonucleotides to the MNPs is performed in a volume of 100 µl. The MNPs are washed twice using a magnetic separator in a washing buffer with 1 M Tris-HCl (pH 8.0), 0.5 M EDTA, polysorbate 20 (Tween-20)(10%) and 5 M NaCl. The MNPs are then re-suspended in 50 µl washing buffer. 6 µl of the oligonucleotide with 1 µM concentration is added to the re-suspended MNPs and the mixture is vortexed and incubated at room temperature for 15 minutes. After the incubation the MNPs are washed again in the washing buffer for two times and re-suspended to the original volume of 100 µl in phosphate-buffered saline (PBS) with a pH of 7.4. With the oligonucleotides bound to the surface, the MNPs are functionalized and can specifically bind to the backbone of the padlock probe amplified by the RCA method.

2.1.4 Detection

In order to detect the RCA products the MNP or fluorescence tags should hybridize to the RCA coils. The functionalized MNPs, tagged with the oligonucleotides, are conjugated to the RCA products by mixing the two samples and incubated the mix for 20 minutes at 55 °C. During the hybridization the sample volume should be kept small in order to increase the chance of the tags and the RCA coils to meet. The samples are then brought to the final desired volume and concentration by adding hybridization buffer solution.

2.1.5 Theoretical and determined RCA concentration

The sample preparation method that is described above gives a theoretical concentration of 5 nM for the RCA products. This value is estimated from the concentration of the padlock probes specified by the vendor. In a recent study by Kühnemund et al. [31], the final concentration of the RCA products in a solution has been determined experimentally. This study shows that the actual number of the products is only 22.6% of the theoretical number. The discrepancy is related to the imprecise determination of the concentration by the vendors, inefficiencies during ligation and amplification reactions.

2.1.6 Monomerized RCA coils

Unlike the PCR method, the RCA amplification is linear and the products are all contained in one continuous DNA molecule. This limited amplification is not sufficient for many applications. However, the circle-to-circle amplification (C2CA) mechanisms can be used to amplify the circular DNA strands without increasing the target analyte concentration [32]. By RCA, a first round of amplification generates large products containing repeated copies of the probe compliment. Through restrictive digestion these large products are cut into monomers. These monomers can then be circularized and ligated for a second round of RCA. An hour of amplification results in 1000 copies of a typical 100 nucleotide long DNA circle. Thus, one cycle of C2CA generates 1000 RCA coils [28]. The C2CA can be preformed several times to achieve a high concentration of RCA coils. Furthermore, the monomerized RCA products can also be used for the detection of the target analyte. The digested RCA products are mixed with two MNP probes with matching motifs on two separate parts of the padlock probe backbone. The presence of the monomers induces agglutination between the two MNP probes by linking them together [33]. The agglutination process aggregates the particles and results in a change in the hydrodynamic size of the MNPs which is detectable through measuring the characteristic relaxation times of the MNPs.

2.2 Magnetic nanoparticles as labels

MNPs are used in a broad field of application including physics, biology and medicine. They are increasingly used in biosensors for their unique properties. They are cheap, biocompatible and have physical and chemical stability [34]. Most biomedical applications of MNPs are thanks to appropriate coating of MNPs with materials that are biocompatible and allow bio-functionalization of the MNPs. A few examples of coatings are polymers, proteins, peptides, oxides, etc [35]. The MNPs we use in our experiments are water/PBS suspended multi-core Fe_2O_3 particles with median diameters of 80 and 100 nm. They are prepared via a core-shell method which embeds

the core magnetite in a non-magnetic shell of hydroxyethyl starch which is a biopolymer material. The coating of these core-shell MNPs with streptavidin enables the bio-functionalization of the MNPs with oligonucleotides.
The specific binding of the functionalized MNPs to the products of the assay, coils or monomers, results in a change in their hydrodynamic size. This change in the hydrodynamic size affects the dynamic properties of the suspended MNP. The effective relaxation time of the MNPs generally describes the dynamics of the particles relating it to the hydrodynamic size, viscosity as well as anisotropy energy [36]. In this section we describe the magnetic relaxation mechanism for the MNPs and ac susceptibility as a method to measure these characteristic relaxation times.

2.2.1 Magnetic relaxation processes

The response of a ferromagnetic material to sudden changes of an external magnetic field shows a time lag. Applying a varying magnetic field to a system of suspended nanoparticles gives rise to relaxation processes that are different from bulk materials. There are two mechanisms responsible for the relaxation of the magnetization of magnetic nanoparticles suspended in a liquid, Fig. 2.2: The Brownian relaxation where the MNPs change their magnetic orientation through a stochastic rotation of the particle itself and the Néel relaxation where the magnetic moment of the particle changes its orientation within the particle overcoming the energy barrier due to anisotropy energy. The time decay associated with rotational diffusion is described by Brownian relaxation time, τ_B:

$$\tau_B = \frac{3\eta V_{hydro}}{k_B T} \tag{2.1}$$

where η is the viscosity of the carrier fluid, $V_{hydro} = \frac{3}{4}\pi r_H^3$ is the hydrodynamic volume of the particle including the core and its shell, k_B is the Boltzman constant, and T is the temperature. The Néel relaxation time, τ_N is given by:

$$\tau_N = \tau_0 \exp(\frac{KV_p}{k_B T}) \tag{2.2}$$

where τ_0 is a material specific characteristic relaxation time, and KV_p is the energy barrier between different directions of easy magnetization.
The Néel relaxation time changes the observed magnetic behaviour of the system with respect to the characteristic experimental measurement time τ_{exp}. If $\tau_{exp} \gg \tau_N$, the system reaches a thermodynamic equilibrium as the relaxation is faster than the magnetization orientation observed. The nanoparticles are then considered to be in a superparamagnetic state. However, for $\tau_{exp} \ll \tau_N$, the particle system is in thermally blocked regime and the magnetization will maintain its direction leading to a quasistatic state in the measurement time window.

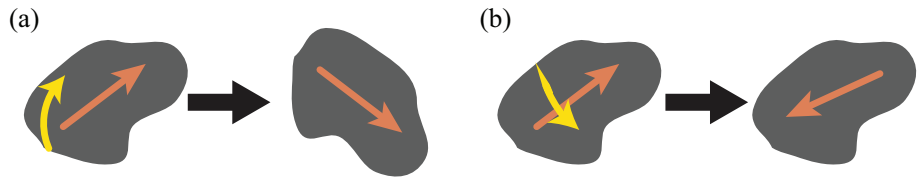

Figure 2.2: Illustration of magnetic nanoparticles relaxation mechanisms: (a) Brownian relaxation due to rotation of the suspended MNP in liquid and (b) Néel relaxation caused by reorientation of the magnetic moment inside the MNP.

The effective relaxation time is, therefore, a combination of the two characteristic times:

$$\frac{1}{\tau_{eff}} = \frac{1}{\tau_N} + \frac{1}{\tau_B} \tag{2.3}$$

and is dominated by the process with the shortest relaxation time. Solving $\tau_N = \tau_B$, for the dimension of the suspended particle determines a critical diameter for the superparamagnetic state [37]:

$$d_{critical} = \sqrt[3]{\frac{6\tau_0 k_B T}{3\pi\eta} \exp \frac{KV_p}{kBT}} \tag{2.4}$$

below and above which the Néel and Brownian relaxation processes are the dominating ones, respectively.
The specific binding of the MNP to the target analyte in our bioassay is detectable through measuring the MNPs' relaxation time. The immobilization of MNPs on large DNA coils changes their hydrodynamic size and according to Eq.(2.1), their Brownian relaxation time. Therefore, the Brownian relaxation should be the dominant process in the suspended MNP system we intend to use in our experiments. In order to assure this, several requirements must be satisfied [37, 38]:

- The thermal energy, $k_B T$, should not exceed the magnetic anisotropy energy barrier, KV_p, of a single particle. If the thermal energy exceeds the energy barrier that separates the easy directions of magnetization, the magnetization will switch direction and give rise to zero net magnetization.
- The diameter of the particles should be larger than the critical diameter, $d_{critical}$, so that the effective relaxation time is essentially dominated by the Brownian relaxation mechanism.
- Comparing the experimental measurement time with the relaxation of internal magnetic moment, τ_{exp} should be shorter than τ_N, in order to distinguish the thermally blocked and superparamagnetic particles.

2.2.2 Ac susceptibility

The Debye theory describes the frequency dependence of complex susceptibility of dispersive materials, such as polar molecules and ferrofluids [39]. This theory holds for spherical particles when the magnetic dipole-dipole interaction is negligible compared to the thermal fluctuations. According to the Debye model, magnetization of a collection of mono-dispersed, non-interaction particles is given by complex susceptibility [40]:

$$\begin{aligned} \mathbf{m}(\omega) &= \chi(\omega) H_{ac}, \\ \chi(\omega) &= \frac{\chi_0 - \chi_\infty}{1 + i\omega\tau_0} + \chi_\infty \end{aligned} \tag{2.5}$$

where $m(\omega)$ is the complex magnetization, H_{ac} is the applied ac magnetic field, τ_0 is the characteristic relaxation time, $\chi(\omega) = \chi\prime(\omega) - i\chi\prime\prime(\omega)$ is the complex dynamic susceptibility and χ_∞ is the high frequency susceptibility. Therefore, the real and imaginary parts of the complex susceptibility are given by:

$$\chi\prime = \frac{\chi_0 - \chi_\infty}{1 + (\omega\tau_0)^2} + \chi_\infty, \tag{2.6}$$

$$\chi\prime\prime = \frac{(\chi_0 - \chi_\infty)\omega\tau_0}{1 + (\omega\tau_0)^2}. \tag{2.7}$$

The real part of the susceptibility decreases with increasing frequency where the imaginary part has a maximum at $\omega\tau_0 = 1$. Assuming that the relaxation process is dominated by the Brownian relaxation process we can assign $\tau_0 = \tau_B$. Fig. 2.3 illustrate the complex susceptibility for 3 particle systems with various particle size that have the Brownian relaxation as the characteristic relaxation process. According to Eq.(2.1), the Brownian characteristic time of these particles depends on their hydrodynamic volume. Therefore, the particle system with greater size (volume) has a longer relaxation time.
In practice, the colloidal magnetic particles have a particle radii distribution. The complex susceptibility then becomes:

$$\chi(\omega) = \int \frac{\chi_0}{1 + i\omega_{eff}(r_H)} f(r_H) dr_H \tag{2.8}$$

where the $f(r_H)dr_H$ is the number of particles with radius between r_H and $r_H + dr_H$ [41]. One commonly used model for the size distribution of the magnetic particles is the so called lognormal distribution:

$$f(r_H) = \frac{1}{\sqrt{2\pi} r_H \ln\sigma} \exp[-\frac{(\ln r_H - \ln \bar{r_H})^2}{2\ln^2\sigma}] \tag{2.9}$$

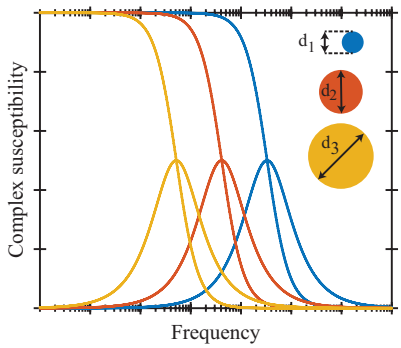

Figure 2.3: Complex magnetic susceptibility for samples with 3 different particle sizes. The imaginary part of the susceptibility maximizes as the frequency approaches the Brownian relaxation frequency for each particle, $\omega_B \tau_B = 1$. Increasing the hydrodynamic diameter of the particles ($d_1 < d_2 < d_3$) shifts the relaxation dynamics to lower frequencies ($\omega_1 > \omega_2 > \omega_3$) and vice versa.

where $\bar{r_H}$ is the median hydrodynamic radius and σ is the standard deviation [42, 43]. By experimentally measuring the complex susceptibility $\chi(\omega)$, it is possible to estimate the distribution of the relaxation time and the particle radii [44].

2.2.3 Cole-Cole plot

Experimental results for the ferrofluid material show that the dispersion of frequency dependent complex susceptibility obeys the following empirical formula:

$$\chi(\omega) = \frac{\chi_0 - \chi_\infty}{1 + (i\omega\tau_0)^{1-\alpha}} \tag{2.10}$$

where τ_0 is the generalized relaxation time, and α can assume values between 0 and 1. Therefore, the real and imaginary part of the complex susceptibility is given by

$$\chi' = \chi_\infty + \frac{1}{2}(\chi_0 - \chi_\infty)[1 - \frac{sinh(1-\alpha)x}{\cosh(1-\alpha)x + \cos\frac{1}{2}\alpha\pi}], \tag{2.11}$$

$$\chi'' = \frac{\frac{1}{2}(\chi_0 - \chi_\infty)\cos\frac{1}{2}\alpha\pi}{\cosh(1-\alpha)x + \sin\frac{1}{2}\alpha\pi} \tag{2.12}$$

where $x = \ln(\omega\tau_0)$ [45]. This equation was developed by two brothers Kenneth and Robert Cole in 1941 [45]. The Cole model can be regarded as a superposition of multiple Debye models with the central relaxation time given by the inverse of frequency of the peak position on the imaginary part of the susceptibility. This

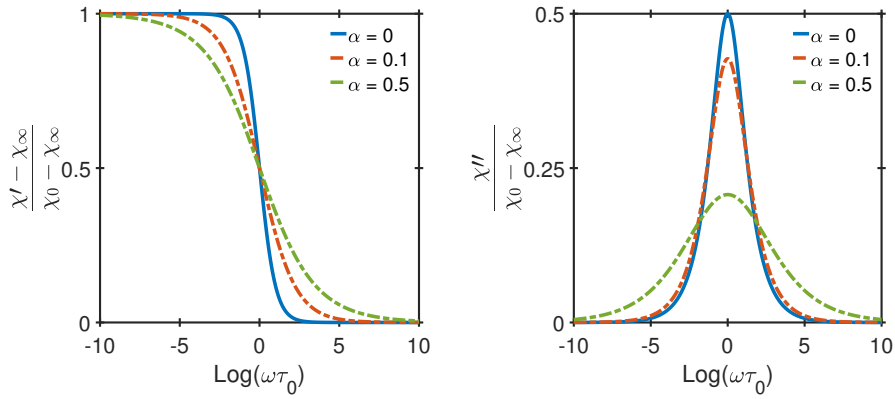

Figure 2.4: (a) Real and (b) imaginary part of complex susceptibility versus frequency for the Debye model Eq.(2.5) and the Cole-Cole model Eq.(2.10). The solid blue curves represent the Debye model and the red and green dashed lines the Cole-Cole model with different $\alpha = 0.1$ and $\alpha = 0.5$ parameters, respectively.

equation reduces to the Debye formula Eq.(2.5) for $\alpha = 0$. For values of parameter α greater than 0, the maximum value of the peak χ'' decreases and the dispersion broadens. Therefore, the α parameter represents the broadness of the relaxation time distribution, Fig. 2.4.
The Kramers-Kronig relations relate the real and imaginary part of the complex susceptibility. Since χ' and χ'' are the conjugate functions, it has been shown that they can be uniquely determined if either one is known over the frequency range [45]:

$$\begin{aligned} \chi'(\omega) &= \chi_\infty + \frac{2}{\pi}\int_0^\infty \frac{\chi''(\nu)\nu d\nu}{\omega^2 - \nu^2}, \\ \chi''(\omega) &= -\frac{2}{\pi}\int_0^\infty \frac{(\chi'(\nu) - \chi_\infty)\omega d\nu}{\omega^2 - \nu^2}. \end{aligned} \tag{2.13}$$

2.3 Magnetic readout

There are various magnetic readout schemes developed for biosensors utilizing MNPs as labels. These methods are based on different techniques and measure either the magnetic permeability to detect the presence of the MNPs, the variation in the hydrodynamic properties of the MNPs, the magnetic flux density change or the change of nuclear spin procession of protons surrounding the MNPs by nuclear magnetic resonance[18]. These techniques are used together with miscellaneous bioreceptors for magnetic biosensing.

Methods based on the variation of the hydrodynamic properties of MNPs use two of the most important characteristic properties of the MNPs: the magnetic signal and the relaxation times. The relaxation mechanisms are affected by the hydrodynamic size of the MNPs and several methods such as magnetic ac susceptibility and magnetic relaxation have been developed to detect this variation. Biodetection by magnetic ac susceptibility was first proposed theoretically by Connolly and St Pierre [41] and was shown experimentally for prostate-specific antigen (PSA) and Brucella antibodies [10, 46]. The detection of the analyte was determined by measuring the change in Brownian relaxation time of the MNPs due to their binding to the target. Many different sensors have been developed that utilize the same principle for detection: SQUIDs [47, 48], differential induction coil system DynoMag (RISE Acreo, Sweden) [10, 30], and opto-magnetic sensors [49, 50]. Some of the magnetic relaxation sensors based on Brownian relaxation have demonstrated promising sensitivities for POC diagnostics. High-T_c SQUID sensors are widely used for their extreme sensitivity to magnetic field and their operating temperature. Using a high-T_c SQUID gradiometer our group has previously demonstrated that in a one-step assay using multi-core particles of 100 nm diameter, we were able to detect PSA molecules with ultimate concentration of 0.7 nM within a 2µL droplet [51, 52]. In this experiment, the biomolecule detection method was an antigen-antibody binding reaction. Chieh et al. [53] developed a magnetoreduction assay that measures the variations in the magnetic properties of marker MNPs under external multiple AC magnetic field excitation to detect the biotarget. Using rf SQUID readout and dextran coated MNP functionalized with c-reactive protein (CRP) antibodies, they have demonstrated an extreme sensitivity of 10^{-6} mg/l to human CRP which is 10^5 times better than the sensitivity of enzyme-linked immunosorbent assay (ELISA) assays. There have also been reports of using the magnetic ac susceptibility measurement technique as a signal transduction method for nucleic acid assays. Examples of this are the volume-amplified magnetic nanobead detection assay using high-T_c SQUIDs [54] and the detection of the *Vibrio cholera* target DNA binding reaction with functionalized MNPs using the commercially available differential induction based high frequency ac susceptometer DynoMag [55]. These results suggest that a sensitive magnetic bioassay can be realized by the right combination of a bio-recognition method and a sensitive magnetic readout.

3

Experimental set-up

In order to reach a very high sensitivity for the bioassay we need to have a sensitive magnetic sensor. SQUIDs are among the most sensitive magnetic field sensors. Therefore, we have developed a SQUID sensor for magnetic measurement of the bio-functionalized MNPs (magnetic markers) in our bioassay. The immobilization of the MNPs to the targets analytes changes their hydrodynamic size. According to Eq. (2.1), this change in size of the MNP affects the Brownian relaxation time. Magnetic ac susceptometry is frequency domain measurement technique and provides high resolution information about the relaxation time and size distribution of the MNPs. In this chapter we describe different components of the experimental set-up used for measuring the ac susceptibility. The set-up consists of a liquid nitrogen cryostat to maintain the high-T_c SQUID sensor at 77 K, a Helmholtz coil to apply external field, an alignment frame for aligning the magnetic field of the Helmholtz coil and a 3D-printed frame for controlling the position of the microfluidic chip above the sensor. The basic principle of the SQUID gradiometer sensor used for magnetic ac susceptometry is explained and the SQUID performance in terms of noise is provided. Microfluidic chips are used to control the sample volume and facilitate sample handling. Sec. 3.2 describes the basics and fabrication of the microfluidic chip. The complete ac susceptibility measurement set-up is described in Sec. 3.3. Finally, simulations of the flux threading the pick-up loops from the ferrofluidic sample are presented and used to study the effect of loop area and channel position.

3.1 Magnetic readout using a high-T_c gradiometer

The 1987 Nobel prize in physics was awarded to J. Georg Bednorz and K. Alexander Müller for the discovering the first high temperature superconductor (HTS) with a transition temperature T_c of 35 K. The same year came the breakthrough of obtaining superconductivity beyond the 77 K, boiling point of liquid nitrogen. The superconductivity in the yttrium barium copper oxide, $YBa_2Cu_3O_{7-\delta}$ (YBCO) compound system was discovered with $T_c = 93$ K [56]. Reproducibility, high quality films and

the low price and abundance of liquid nitrogen as the refrigerant are the most significant advantages of the YBCO superconductor making it one of the most commonly used high-T_c superconductors today. This section describes the basic principle, operation and performance of the high-T_c SQUID gradiometer, which is used in our biomagnetic read out set-up.

3.1.1 dc-SQUID

Josephson junctions are active devices in superconductive electronics. They consist of two superconductors separated by a weak link. The weak link should only allow a slight overlap of the electron pair wave function of the two superconductors. There are many ways to form these weak links in HTS. Three of the most standard methods are bicrystal grain boundary junctions, step-edge junctions and ramp edge junctions [57]. The Josephson relations govern the behavior of such a device [58]:

$$\begin{aligned} I &= I_c \sin(\phi) \\ \frac{\partial \phi}{\partial t} &= \frac{2e}{\hbar} V = \frac{2\pi}{\Phi_0} V \end{aligned} \tag{3.1}$$

where I_c is the critical current, ϕ is the superconducting phase difference across the junction, e is the electron charge and $\Phi_0 = \frac{h}{2e} = 2 \times 10^{-15}\ Wb$ is the flux quantum. Since the phase difference across the weak link can be varied by the magnetic field passing through it, the critical current depends also on the magnetic field or the flux threading the junction :

$$I_c(\Phi) = I_c(0) \left| \frac{\sin(\pi \Phi / \Phi_0)}{(\pi \Phi / \Phi_0)} \right|, \tag{3.2}$$

where $I_c(0)$ is the maximum critical current. The total critical current as a function of applied flux is plotted in Fig. 3.1.
The dc-SQUID is a superconducting loop which contains two Josephson junctions and combines the flux quantization and Josephson effects, Fig. 3.2. The relation between the phase differences across the two junctions changes if a magnetic flux is threading the loop. Therefore, similar to the single Josephson junction the total critical current of the dc SQUID is a function of applied flux in the superconducting loop, Fig. 3.2 (b). Assuming the critical current of the two junctions to be the same, $I_{c1} = I_{c2} = I_c$, and the SQUID inductance is negligible, the total critical current becomes:

$$I_{Tc}(\Phi) = 2I_c \left| \cos\left(\frac{\pi \Phi}{\Phi_0}\right) \right|. \tag{3.3}$$

A typical current-voltage characteristic of a dc SQUID in an external magnetic flux is illustrated in Fig. 3.3(a). Here we have the two extreme cases where the values

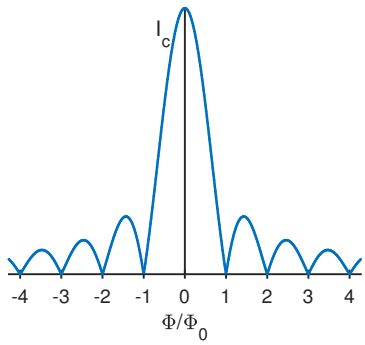

Figure 3.1: Dependency of the Josephson junction critical current on external applied flux.

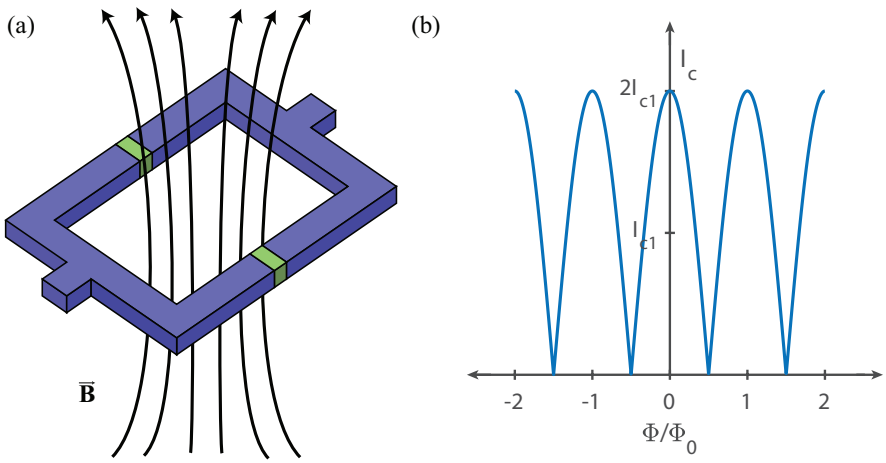

Figure 3.2: (a) A dc SQUID with two Josephson junction interrupting the superconducting ring. (b) The dependence of total critical current of a dc SQUID on external magnetic flux.

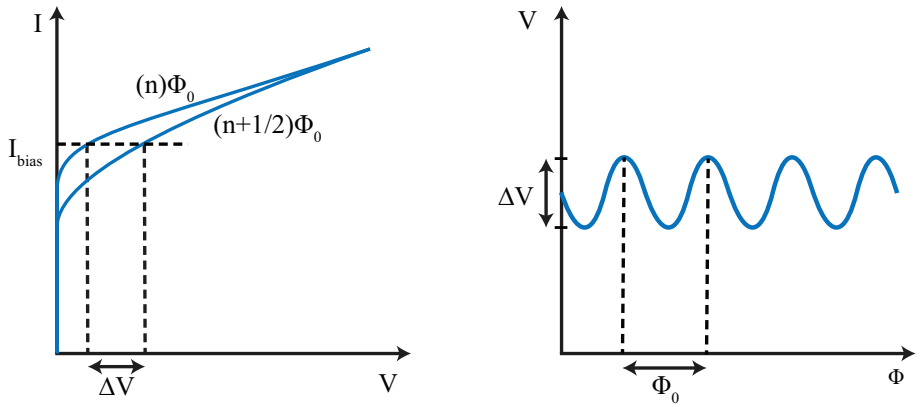

Figure 3.3: (a) The current-voltage characteristics of a dc SQUID for integer and half-integer multiples of applied flux quantum
;(b) voltage versus applied external flux for an applied constant bias current, with $I_{c1} = I_{c2}$.

of applied flux is integer or half-integer. To operate the SQUID, a constant bias current I_b is applied. If the SQUID bias current is slightly higher than the critical current of the SQUID, $I_b > I_c$, the junctions are in the voltage state (a voltage appears across the junctions), while the critical current of the junctions is modulated by the external flux. In this case, any change in the applied external flux induces a screening current that adds to the bias current through the junctions. When the applied flux reaches half a flux quantum, $\Phi = \Phi_0/2$, we are at the minimum critical current of the SQUID and a flux quantum enters into the ring changing the direction of the screening current. As the external flux increases to a flux quantum the critical current reaches its maximum again. The voltage drop across the SQUID in turn swings between the two extreme cases as a function of external flux with period of Φ_0, Fig. 3.3(b). SQUID is therefore a flux-to-voltage transducer and the maximum response to a small change in the applied flux is obtained where the flux-voltage transfer function $V_\Phi \equiv |(\Delta V/\Delta\Phi_{ext})_{I_b}|$ is at a maximum.

3.1.2 dc SQUID gradiometer

A wide range of input circuits can be coupled to the dc SQUIDs for various applications. In order to measure extremely weak magnetic fields a flux pick-up loop configured as a magnetometer or gradiometer is coupled to the SQUID. Both the SQUID magnetometer and gradiometer are only sensitive to the variation of the magnetic field rather than measuring the absolute field strength. For our biomagnetic measurements, we would like to operate the SQUID outside a magnetically

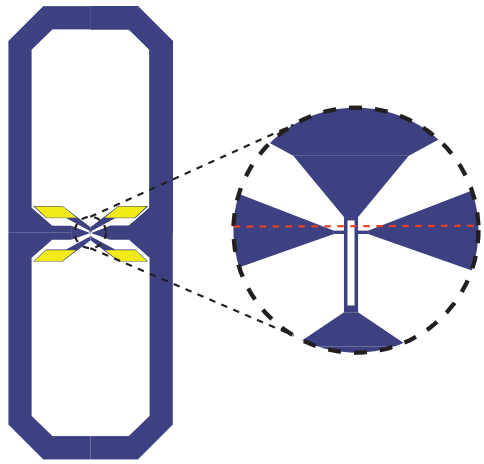

Figure 3.4: The layout of the fabricated gradiometer with 3.6 mm baseline. The width of the pick-up loops are 400 µm. The red dashed line indicates the bicrystal grain boundary, which creates the Josephson junctions in the superconducting SQUID loop. The SQUID loop has 4 µm wide striplines and the length and width of the slit are 50 µm and 3 µm, respectively.

shielded room and apply a homogeneous magnetic field from a Helmholtz coil in the vicinity of the SQUID. Therefore, the gradiometer layout is more appropriate option for a sensor because it allows the magnetic field source to be close to the SQUID and it discriminates against distant magnetic sources.
The layout of our SQUID gradiometer is shown in Fig. 3.4. The baseline of the gradiometer, connecting the center of the two superconducting pick-up loops, is 3.6 mm. The screening currents induced by a homogeneous field in each of the two pick-up loops cancel each other in the center line of the loop. The SQUID is placed in the center of the middle line. The SQUID is directly connected to the pick-up loops and therefore can sense only the difference in magnetic flux in them. The SQUID is made from bicrystal grain boundary junction in YBCO film; the fabrication technology is comprehensively described in earlier work [59, 60].

3.1.3 SQUID readout

Since the SQUID has a non-linear voltage-flux response, it has to be operated in a so called flux locked loop (FLL) readout scheme. The SQUID is flux biased using an external coil at a working point where the slope of the voltage to flux modulation is the steepest. In order to lock the SQUID at this working point, the output voltage of the SQUID is amplified and a flux is fed back into the SQUID through an integrator, a feedback resistor (R_f) and via a feedback coil inductively coupled to the SQUID.

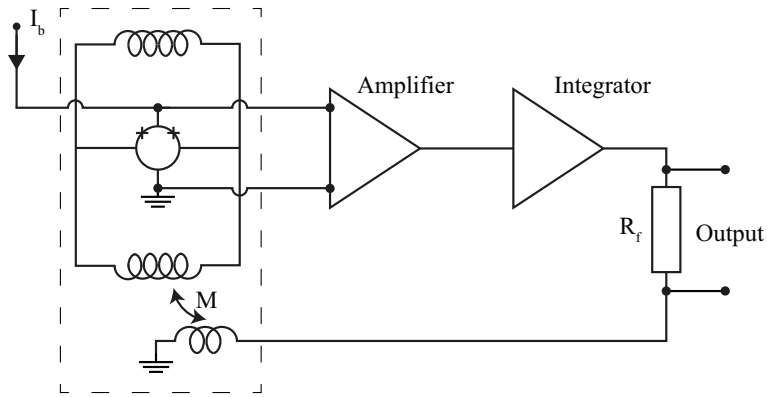

Figure 3.5: Basic flux locked loop circuit with direct readout of the SQUID. The SQUID voltage is amplified and integrated and is sent back to the feedback coil which is inductively coupled to one of the gradiometer loops. The output voltage measured across the feedback resistor is proportional to the feedback current that keeps the total flux in the SQUID loop constant. The voltage therefore, linearly depends on the applied flux. Components which are at liquid nitrogen temperature are inside the dashed box.

The feedback flux compensates the applied external flux signal to the SQUID and the voltage across the feedback resistor gives the output voltage (V_{out}) that now depends linearly on the applied external flux signal, Fig. 3.5.

The performance of the SQUID at low frequencies, however, may be limited by $1/f$ noise. There are two major contributors to the $1/f$ noise in HTS SQUIDs: one is the motion of trapped flux in the superconducting film and the other one is fluctuations of the critical current in the Josephson junctions. The former can be minimized by improving the pinning of the vortices inside the superconductor and to avoid vortex penetration. The later is the dominant source of low-frequency noise in high-T_c SQUIDs. The critical current fluctuations appear either as a voltage across the SQUID or as a flux in the SQUID and are defined as in-phase and out-of-phase contributions. The flux modulation readout with constant bias current easily suppresses the in-phase contribution, while the out-of-phase fluctuations remains a problem as it cannot distinguish applied flux from the out-of-phase fluctuations. The two can be discriminated by reversing the bias current. When the SQUID is positively biased, the applied flux and out-of-phase fluctuations have the same effect, however, they show an opposite effect for reversed bias current. Therefore, by applying a bias current reversal scheme which switches between positive and negative bias current, the net effect of the out-of-phase fluctuations can be eliminated on every period of bias reversal [57].

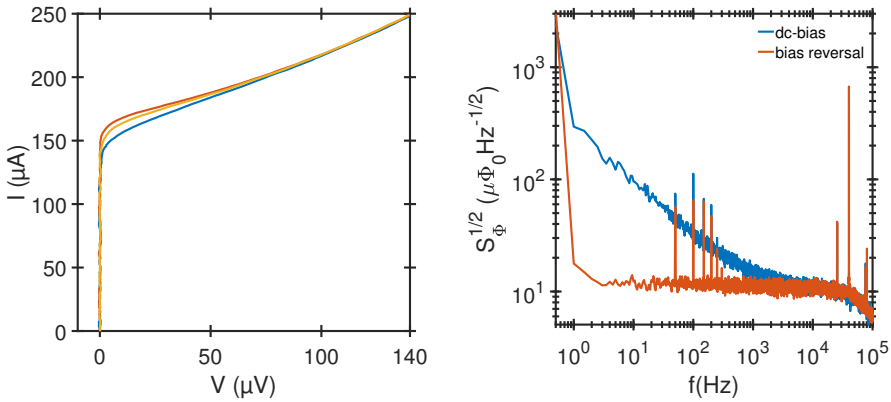

Figure 3.6: (a) Flux modulated IV characteristics of the SQUID with a critical current of 170 µA at 77 K. The maximum voltage modulation is 16 µV. (b) Flux noise of the SQUID gradiometer measured inside a magnetically shielded room. The blue curve with the high $1/f$ noise was measured using dc-bias. The low frequency noise is suppressed by using bias reversal as can be seen in the red curve.

3.1.4 Sensor performance

The SQUID gradiometer chip is glued on to a sapphire rod in direct contact with the liquid nitrogen bath and electrically connected to the amplifiers through a break-up box. The cryostat is placed inside a magnetically shielded room and the I-V characteristics of the SQUID are measured. Fig. 3.6(a) shows the flux-modulated I-V characteristics of the SQUID. The flux noise of the SQUID gradiometer is also measured inside the magnetically shielded room in dc bias and bias reversal modes. The best white noise level achieved for this device is 12 $\mu\Phi_0/\sqrt{Hz}$. As can be seen in Fig. 3.6(b), the $1/f$ noise due to critical current fluctuations is suppressed in the bias reversal mode.

3.2 Fabrication of microfluidic channels

Microfluidic technology has shown the potential to significantly improve the diagnostic research. There are many advantages in using microfluidics specially for standard laboratory set-ups, e.g. sample processing and precise control of fluids. This is extremely important particularly when small sample quantities are available for traditional experimental bio-analysis approaches. Handling small volume of samples make it possible to develop systems that are more compact and portable, and promises the automation of chemistry and biology [61, 62].

There are different materials that are used to fabricate microfluidic devices for instance, poly(dimethylsiloxane) (PDMS), silicon, glass, etc. We have chosen PDMS for our microfluidic chip for its fast, easy and cost effective fabrication process. It is nontoxic, biocompatible, durable and flexible, which makes it a great candidate for future POC developments [63]. PDMS devices are fabricated using soft lithography. There are different methods to fabricate the master mold for casting replicas, such as photolithography, wet etching, wet/dry silicon etching, etc. Since the microfluidic devices being used here are rather simple and have large features, precision machining has been used to fabricate the microfluidic devices. The main advantage of this technique is the fast transfer of a computer aided design (CAD) into a finished device. The elastomeric material PDMS, is used as the casting material, which is very flexible, cheap, nontoxic and easy to handle [64]. The molecular chains in the elastomer are long and entangles but show no chemical interaction. The structure of the channel is precision machined into a master aluminum piece and many copies of the device are made from the same mold with good accuracy using the elastomer PDMS. Fig. 3.7 shows the dimensions of the microchannel with 1×1 mm^2 channel cross-section and a photograph of completely fabricated chip.
Before the microfluidic channel is functional the chips are required to be closed. The molding creates a PDMS replica with three of the four walls necessary to have an enclosed channel and since we would like the samples to be as close as possible to the sensor, a thin layer of PDMS is used to close the channels. A 100 µm thin layer is spin coated on a silicon wafer and heat cured. Then the capping layer and the PDMS replica are put together to close the channel since surface adhesion of the PDMS is normally sufficient to create a good contact. To make sure we have a tightly enclosed channel that does not leak under pressure, the two surfaces of the PDMS and the capping layer are primed in oxygen plasma before they are brought into contact. This process increases the bonding strength and can lead to a permanent bond between the two by forming covalent bonds [65].

3.3 Ac susceptibility set-up

The following section describes different parts of the the experimental set-up for the biomagnetic assay. These different parts include a cryostat for operating the SQUID at 77 K, excitation coils and alignment system to apply external magnetic field for ac spectrometry and microfluidics for handling the biological samples. Fig. 3.8 shows a photograph of the experimental set-up.
The SQUID gradiometer is operated inside a cryostat fabricated in-house. The cryostat is made from nonmagnetic materials. The sensor chip sits on a sapphire rod in direct contact with the liquid nitrogen. The liquid nitrogen reservoir is made out of fiber glass is thermally decoupled from the environment by vacuum. A 250 µm thick sapphire window on the polyvinyl chloride (PVC) vacuum shell separates the

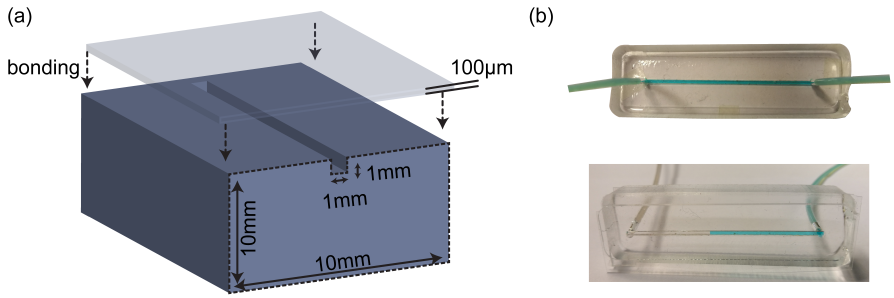

Figure 3.7: (a) The dimensions of the microfluidic channel and (b) a photograph of completed PDMS chip enclosed by bonding a 100 µm thin PDMS cap layer.

77 K vacuum enclosed environment of the SQUID sensor from the room temperature environment. The distance from the sensor to the top of the sapphire window is less than 1 mm to allow strong coupling between the biomagnetic samples and the superconducting pick-up coils of the gradiometer.
A Helmholtz coil with 20 turns and radius of 15 cm is used for producing a homogeneous magnetic field to excite MNPs. The Helmholtz coil is placed on a movable frame and is manually aligned in order to minimize the coupling between the excitation field and the pick-up loops of the SQUID. The microfluidic chip is placed on the sapphire window for handling the samples. A peristaltic pump connected to reservoirs allows pumping a small sample volume to the microfluidics channel, which is aligned to sit above the sensitive part of the pick-up coils of the SQUID gradiometer, see Sec 3.4.2.1. Therefore, an alignment frame was designed which allows moving of the microfluidic chip in the X-Y plane of the sapphire window above the SQUID. Fig. 3.9 shows the designed frame, which is 3D-printed and mounted on the cryostat.

3.3.1 Ac susceptometry with SQUID gradiometer

Ac susceptometry is used to measure the change in size distribution of the MNPs. The measurement technique involves magnetization of MNPs by an external ac magnetic field and measuring the magnetization of the MNPs by the SQUID, see Sec. 2.2.2. The ac susceptibility measurement set-up is shown in Fig. 3.8. A fluke AWG-220 waveform generator drives the Helmholtz coil creating a sinusoidal external excitation field. The sample is pumped into the microchannel sitting on the sensitive part of the SQUID gradiometer sensor. The SQUID signal is read out by Magnicon SEL-1 electronics in FLL mode. A Stanford SR-830 lock-in amplifier is used to extract

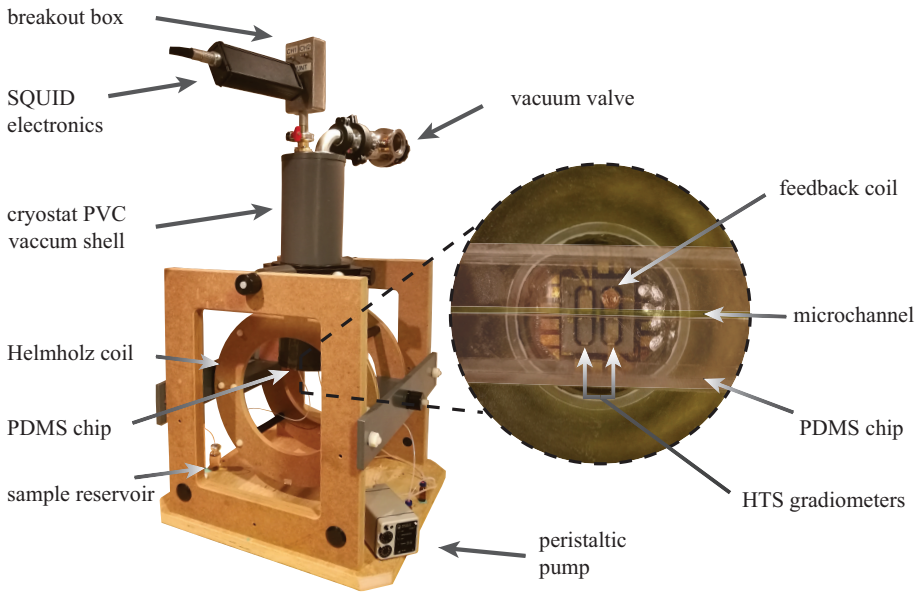

Figure 3.8: A photograph of the experimental set-up and a close up top view of the microchannel on the sapphire window. The SQUID is located under the 250 µm thick sapphire window and the Helmholtz coil is aligned so that the SQUID is at the center of the coil with highest field homogeneity. The small volumes of target analyte and MNPs are then pumped in and out of the microchannel using the peristaltic pump.

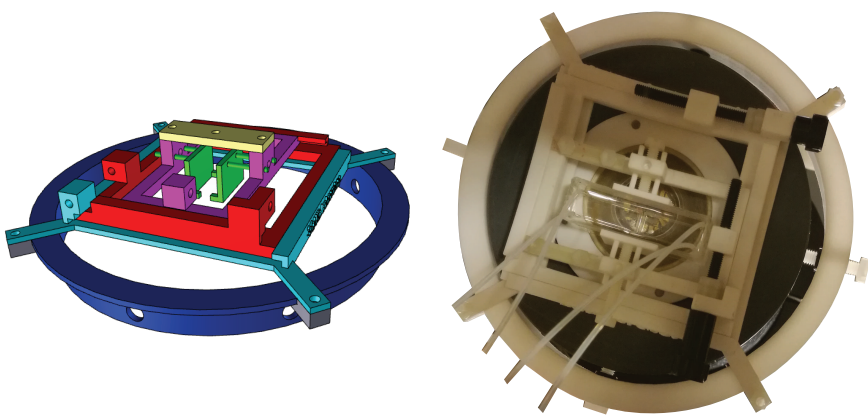

Figure 3.9: An illustration of the designed microfluidic chip frame for precise alignment of the chip on the sensitive part of the sensor. A photograph of the 3D-printed frame mounted on the cryostat holding the PDMS chip on the sapphire window above the SQUID sensor.

the real and imaginary components of the magnetic susceptibility from the SQUID gradiometer signal having the excitation frequency as a reference. The excitation field is in the range of 1 Hz to 10 kHz. In order to eliminate the residual coupling of the excitation field to the pick-up coils, a calibration measurement is made without having any samples. This calibration is considered the background and is subtracted from all measurements with MNPs leaving only the response from the samples.
Upon binding of the MNPs with the RCA products, the hydrodynamic size of the MNPs change and the frequency corresponding to the Brownian relaxation time of the MNP changes, Fig. 2.3. Extracting the frequency and amplitude of the imaginary susceptibility for the MNPs with and without any biological target can be used as the parameter for the detection of the biological target. Introducing the target analyte and specific binding of MNPs to it consequently changes the detection parameter, i.e. the frequency and amplitude of the imaginary susceptibility.

3.4 Simulation

We evaluate the flux threading a pick-up loop produced by a MNP and calculate the magnetic response from the MNP as a function of its positions within the pick-up loop. First, we start with a single MNP and then we extend the calculation to the flux from several hundreds of MNPs which are randomly distributed in the volume of a microchannel. The MNP is considered a point-source particle with magnetic moment $\mathbf{m}$ oriented at a random direction and placed at point $\mathbf{r_0}$. The dipole field from the MNP at point $\mathbf{r}$ is:

$$\mathbf{H}(\mathbf{r}) = \frac{1}{4\pi}\left(\frac{3(\mathbf{r}-\mathbf{r_0}) - m\cdot(\mathbf{r}-\mathbf{r_0})}{|\mathbf{r}-\mathbf{r_0}|^5} - \frac{\mathbf{m}}{|\mathbf{r}-\mathbf{r_0}|^3}\right). \tag{3.4}$$

More succinctly, we can define the dipole vector potential of the MNP at point $\mathbf{r}$ as:

$$\mathbf{A}_{dip} = \frac{\mu_0}{4\pi}\frac{\mathbf{m}\times(\mathbf{r}-\mathbf{r_0})}{|\mathbf{r}-\mathbf{r_0}|^3} \tag{3.5}$$

and the magnetic flux threading the pick-up loop is

$$\phi = \oint \mathbf{A}_{dip}\cdot d\mathbf{l} \tag{3.6}$$

where the integral is over the closed line of the pick-up loop, Fig. 3.10. In a field range where the magnetic response of the particle is linear, the applied magnetic field is much lower than the saturation field of the particles, the particles orient themselves along the field lines. Having the magnetic moment of the MNP oriented along the applied external field, the integral Eq.(3.6) provides the magnetic flux distribution threading the pick-up loop as a function of the MNP's position with respect to the loop. Summing all the flux contributions from every single MNP gives the total flux

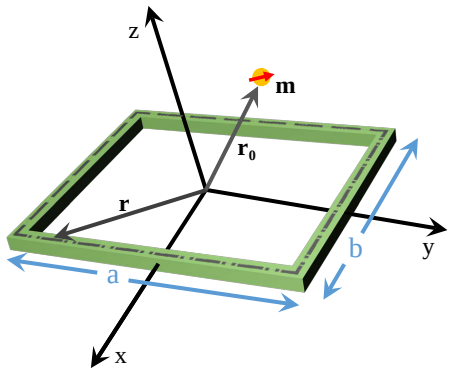

Figure 3.10: Illustration of a single pick-up loop and the definition of coordinate system and geometries.

from the colloidal MNP sample threading the pick-up loop. In the following sections, we first calculate the flux from a single MNP threading a loop to provide an overall picture of flux distribution as function of MNP position and excitation field direction. We extend the simulations further by creating a particle system of hundreds of MNPs randomly distributed within the geometry of our microfluidic channel and study the flux threading the gradiometer sensor as a function of microchannel position.

3.4.1 A single point-source MNP

The MNPs inside the fabricated microchannel are distributed homogeneously inside the volume of the channel. However, to make the simulations easier, we only assume a single MNPas a point-source. In the following simulations we also assume that: (I) the particle-particle interaction can be neglected, (II) the MNPs are thermally blocked with constant magnetic moment, (III) the film thickness of the pick-up loops is neglected and (IV) the external magnetic field magnetizes all the MNPs towards the applied field direction and therefore, the point-source magnetization is also aligned with the field. In the next section, we use randomly distributed MNPs in a volume and sum all the flux contributions from every single MNP to calculate the total flux from the colloidal MNP sample threading the pick-up loop. This also makes it possible to study the effect of the channel geometry on the flux threading the pick-up loop.
For simplicity, we first calculate the flux threading a single loop. The magnetic moment of the MNPs with median size of 100 nm is about 4.8×10^{-22} Am^2 [1], and

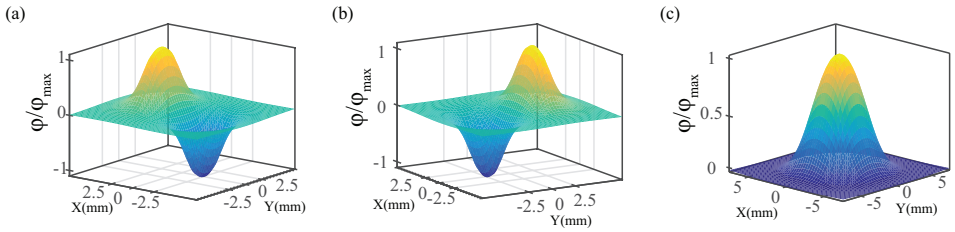

Figure 3.11: Normalized flux distribution from a point-source MNP at constant distance of 1.1 mm from a sensing coil of 5 by 5 mm, sweeping the plane of the coil. The magnetic excitation is in (a) x, (b) y and (c) z direction.

for the following simulations we assume we have 10^6 MNPs agglomerated to form a single point-source MNP. The applied homogeneous magnetic field is aligned in x, y and z directions magnetizing the point-source towards the field direction. Placing the point-source MNP on the plane of the 5×5 mm^2 square loop with constant distance z_0, and integrating Eq.(3.6) over the closed line of the sensing coil, we calculate the flux threading the coil. Fig. 3.11 shows the normalized magnetic flux distribution $\frac{\Phi(\mathbf{r_0})}{\Phi_{max}(\mathbf{r_0})}$ produced by this point-source MNP threading the loop for external applied field along x, y and z directions. The point-source sweeps the x-y plane and at each point the flux threading the sensing coil is calculated. The color coding represents the normalized amplitude of magnetic flux ϕ/ϕ_{max} at each point.

For an applied magnetization field in the x or y direction, the maximum flux from the dipole field of the point-source MNP is given when the particle is on the orthogonal side lines of the sensing coil. If the applied magnetization is in z direction, placing the magnetic particle at the center of the coil gives the maximum flux threading the sensing loop. Since the excitation field of the Helmholtz coil is in plane of the gradiometer sensor, the x and y magnetization are the relevant cases and we will only study these two excitation directions.

Another parameter that is of interest is the area of the sensing coil. The maximum magnetic flux threading the loop is calculated for an excitation field applied in either the x or y direction and the results are shown in Fig. 3.12. The maximum flux is calculated at different distances from the plane of the sensing coil versus the coil area. For all distances to the coil plane, the flux increases with increasing loop size, however, the maximum flux saturates for a particular area of the loop and it does not depend on the area anymore. Thus, the maximum flux threading the loop not only depends on the position of the point-source MNP but also on the size of the pick-up loop area.

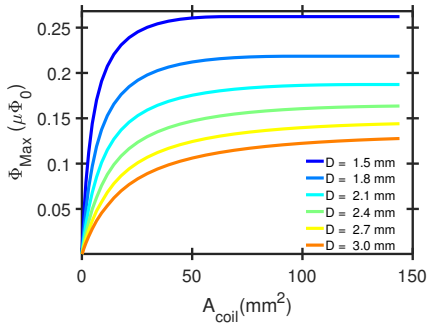

Figure 3.12: Maximum flux from a point-source MNP versus the area of the sensing loop for an excitation field in y direction and different distances between the MNP and the plane of the loop.

3.4.2 Magnetic flux from a colloidal solution of MNPs

In reality the MNPs are not aggregated into a point-source but are suspended in the volume of the microchannel. As it is evident from Fig. 3.12, at a constant loop area the flux threading the loop decreases as nanoparticles move away from the plane of the coil. In a colloidal sample, some of the MNPs are at the bottom of the channel while some are furthest away on the top, therefore, it is more realistic to study the magnetic flux through the pick-up coil due to a random distribution of suspended particles in liquid. In order to simulate this colloidal solution, the MNPs are randomly distributed in the $1 \times 1 \times 3$ mm^3 volume of the microchannel. Fig. 3.13(a) illustrates the distribution of 100 MNPs inside the volume of the microfluidic channel, where the bottom of the microchannel is placed at 1.1 mm distance from the plane of the sensing loop. This is the physical distance between the SQUID sensor and the bottom of the microfluidic channel. Having the magnetic excitation in the y direction the flux distribution from the colloidal sample is calculated by summing the integral Eq.(3.6) over the closed line of the coil for every single MNP inside the volume of the channel, Fig. 3.13(b).

3.4.2.1 Magnetic flux of a colloidal sample threading a gradiometer

The sensor layout that we use does not have a single pick-up loop and is a first order superconducting gradiometer which basically measures the difference in the flux lines threading each loop. We have simulated the magnetic flux threading our gradiometer sensor, Sec. 3.1.2, for a randomly distributed MNPs in $1 \times 1 \times 3$ mm^3 volume with the bottom of the channel in plane with the gradiometer at a distance of 1.1 mm. Fig. 3.14 shows the absolute value of the normalized flux difference $|\frac{\Phi_1 - \Phi_2}{(\Phi_1 - \Phi_2)_{max}}|$ in the two loops of the gradiometer versus the position of the microchannel.

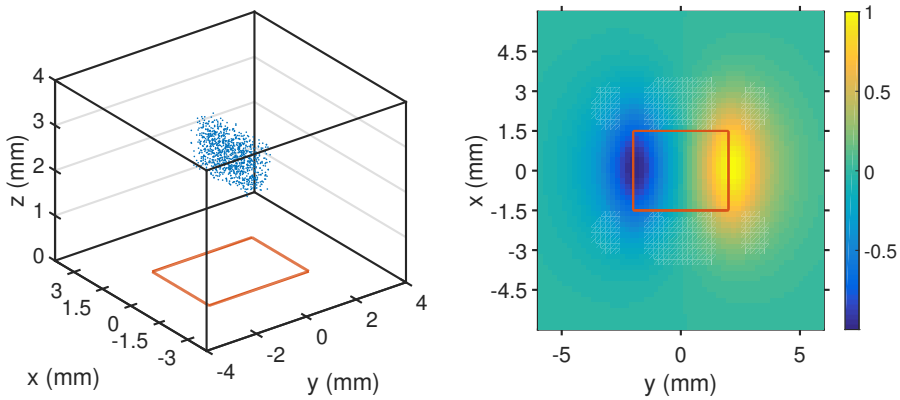

Figure 3.13: (a) Random distribution of MNPs in the 1 by 1 by 3 mm^3 volume of the microchannel at a constant distance of 1.1 mm above the plane of the 3 by 4 mm^2 sensing loop. (b) Magnetic flux from the same sample threading the sensing loop versus the position of the channel with the excitation field in the y direction.

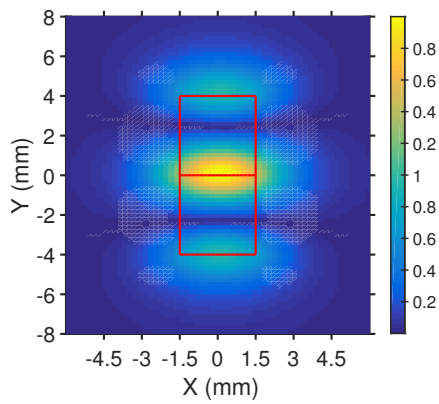

Figure 3.14: Absolute total flux difference threading the gradiometer sensor from a colloidal sample in a microchannel of 1 by 1 by 3 mm^3 volume. The center of the channel sweeps the x-y plane of the gradiometer at a constant distance of 1.1 mm and the flux at each point is normalized to the maximum flux difference in the gradiometer loops with the excitation field in y direction.

The results show that to have the maximum signal from the sample, the channel should be placed at the center line of the gradiometer. In this case, the magnetization field lines from the sample go in the loop one and out of loop two and have opposite signs. Since the gradiometer subtracts the fluxes from the two loops they add up and we get the maximum flux from the sample at the center line of the gradiometer.

4

Experimental Results

In this chapter, the experimental results from characterization of the MNPs and the SQUID sensitivity to iron content are presented. The limit of detection (LOD) to target analyte, the RCA coils, is estimated from magnetic ac susceptibility measurements. The results include measurements of RCA coils and the agglutination of MNPs with monomers from digested RCA coils.

4.1 Characterization of MNPs and system sensitivity

The ac magnetic susceptibility technique, as described in Sec. 2.2.2, is used to characterize the MNPs. The volume and geometry of the magnetic fluid is fixed to 3 µl in volume using the microfluidic channel, Sec. 3.2. The filled channel is placed above the most sensitive part of the gradiometer, and an external ac magnetic field with frequency range of 1 to 10 kHz and field strength of 40 µT is applied to the sample. The signal is measured using the SQUID gradiometer sensor. The MNPs used in this part are the streptavidin-coateded MNPs with a median size of 100 nm from Micromod (Micromod Partikeltechnologie GmbH, Rostock, Germany). The in-phase and out-of-phase component of the SQUID signal acquired from samples of various concentrations diluted in PBS versus the excitation field frequency are shown in Fig. 4.1. The in-phase and out-of-phase components are related to the real and imaginary components of the ac susceptibility, respectively. The imaginary part of the susceptibility peaks at the Brownian relaxation frequency at around 80 Hz, which corresponds to the median particle size of 100 nm according to Eq.(2.1). The empirical Cole-Cole formula, Eq.(2.10), is used to accurately find the frequency of the imaginary ac susceptibility peak. The amplitude of both real and imaginary parts of the susceptibility decreases with decreasing the concentration of MNPs. There is no frequency shift in the peak position of the imaginary part. Any shift in the position of this peak frequency would translate into a change in the hydrodynamic size of the MNPs, Eq.(2.1).
In order to extract the iron content sensitivity, different concentrations of the mag-

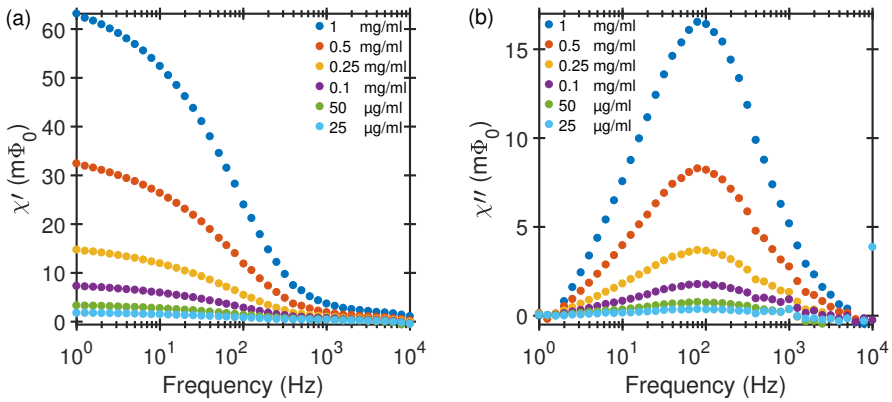

Figure 4.1: (a) In-phase and (b) out-of-phase components of SQUID signal versus the excitation field frequency for different concentrations of streptavidin-coateded MNPs. Magnetic field strength is 40 µT. The in-phase and out-of-phase components are related to the real and imaginary components of ac susceptibility, respectively. The imaginary ac susceptibility peak position is at 80 Hz.

netic fluid with a constant volume of 3 µl was measured. Six different concentration, from 1 mg/ml to 25 µg/ml of MNPs per unit volume were measured. The number of MNPs in each concentration is estimated from the known number of particles per unit volume: 6.0×10^{12} particles per ml in a 10 mg/ml concentration.
Fig. 4.2 shows the linear relation between the amplitude of the peak out-of-phase component and the number of MNPs. The vertical axis corresponds to the SQUID output signal in the units of magnetic flux quanta. The extrapolation of this linear dependence to the measured noise floor of the SQUID, $1.2 \times 10^{-5}\Phi_0/\sqrt{Hz}$, gives the estimation of the magnetic content sensitivity of our system to be $1.5 \times 10^6 MNPs/\sqrt{Hz}$ or $2.9 \times 10^{-10} emu/\sqrt{Hz}$ in magnetic moment. This is equivalent to 2.5 ng of MNP. This value is an important figure of merit as it is used to determine the sensitivity of the magnetic bioassay.

4.2 Stability of the MNPs solutions

A sensitive biomagnetic assay with high sensitivity and specificity requires streptavidin-coated MNP system which is colloidally stable. Measuring on samples with streptavidin-coateded MNPs inside the microfluidic channel showed a loss of signal over time. This loss of signal could be caused by either agglomeration of the streptavidin-coateded MNPs, sedimentation of the particles inside the channel, or binding of the MNPs to the surface of the PDMS channel. This phenomenon, however, was not observed

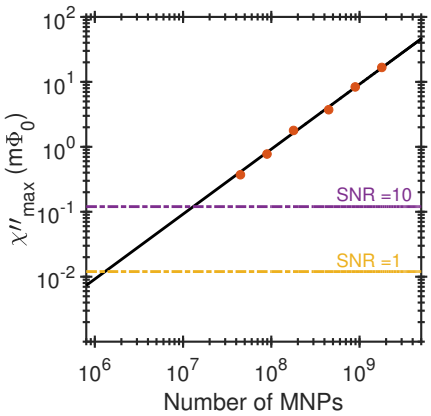

Figure 4.2: The measured maximum out-of-phase signal as a function of number of MNPs. The dashed-dotted lines are the signal to noise ratio (SNR) of 1 ($1.2 \times 10^{-5}\Phi_0/\sqrt{Hz}$) and 10 ($1.2 \times 10^{-4}\Phi_0/\sqrt{Hz}$).

for uncoated-MNPs. Since the reduction in the imaginary component of the ac susceptibility is the parameter we measure in order to detect the target analyte, any instability in the colloidal solution would cause an error in the measurement, particularly at very low target concentrations.
In order to study the stability of the samples, we have measured the ac susceptibility of both uncoated and streptavidin-coateded MNPs, Fig. 4.3. The channel was filled with the fluidic sample and the ac susceptibility was measured 3 times without moving the sample inside the microchannel. The results shows no substantial shift in the peak frequency of the imaginary component and therefore the hydrodynamic size of the MNPs has not changed or changes slower than the measurements time window of the three subsequent measurements. There is, however, still some signal loss, which is more pronounced in streptavidin-coateded MNPs than in the uncoated-MNPs.
To see the dynamical behaviour of this signal loss, the real and imaginary part of the ac susceptibility at a frequency close to the peak amplitude of imaginary part was measured for a duration of 12 minutes. The data points were taken every second for both uncoated-MNPs and coated-MNPs and are plotted against time in Fig. 4.4 (a) and (b), respectively. For the sample containing the uncoated-MNPs with median size of 80 nm and concentration of 0.5 mg/ml both components of the ac susceptibility were measured at a frequency of 251 Hz. The two ac susceptibility components change very insignificantly with time during the measurement. Measuring the ac susceptibility of the streptavidin-coateded MNPs with 100 nm median size and 1.0 mg/ml concentration at a fixed frequency of 63 Hz as a function of time, however, shows a continuous decrease. This constant decrease in signal with time is an issue which needs to be addressed if the particle system is to be used as markers in

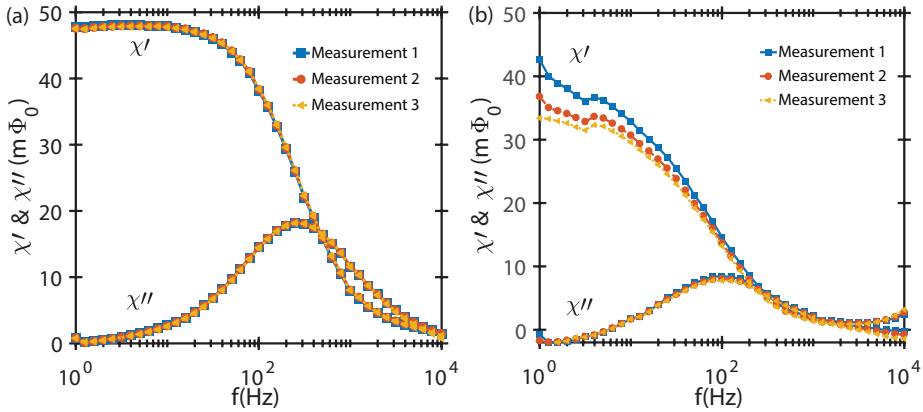

Figure 4.3: Three consequent measurements of magnetic ac susceptibility for (a) uncoated-MNP and (b) streptavidin-coated MNPs in the microfluidic channel.

biomagnetic assays.
Slopes of the lines in Fig. 4.4 define if the signal is increasing or decreasing over time. The slope for both the real and imaginary component of the ac susceptibility from the uncoated-MNPs is around 90 nV/s and positive. This means that it takes roughly 40 hours for this rate of change to affect the signal and increase it by 1%. The slopes for the streptavidin-coateded MNPs are much larger and are roughly -1.12 µV/s and -0.75 µV/s for real and imaginary components, respectively. Therefore, it takes 2.5 and 3 minutes for the real and imaginary components of the ac susceptibility to lose 1% of the signal, respectively. This is a much higher rate compared to the uncoated-MNPs. This signal loss can be attributed to the streptavidin-coateding of the 100 nm MNPs since the two particle system are the same otherwise. Streptavidin tends to bind to the surface of the PDMS channel [66] that may result in the loss of the signal. A possible solution is to coat the microfluidic channel with biocompatible materials such as poly(ethylene oxide) (PEO) and poly(ethylene glycol) (PEG) to avoid nonspecific binding of the streptavidin-coated MNPs to the surface [67].

4.3 Detection of RCA coils and determination of target analyte limit of detection

The assay that is used in the following experiments is fully described in Sec. 2.1. The final product of this assay is large DNA coils that have the sequence that can be conjugated with the detection oligonucleotides. Upon hybridization of the oligonucleotide-functionalized MNPs with these DNA coils, the hydrodynamic size of the MNPs increases, and therefore their Brownian relaxation time changes. This

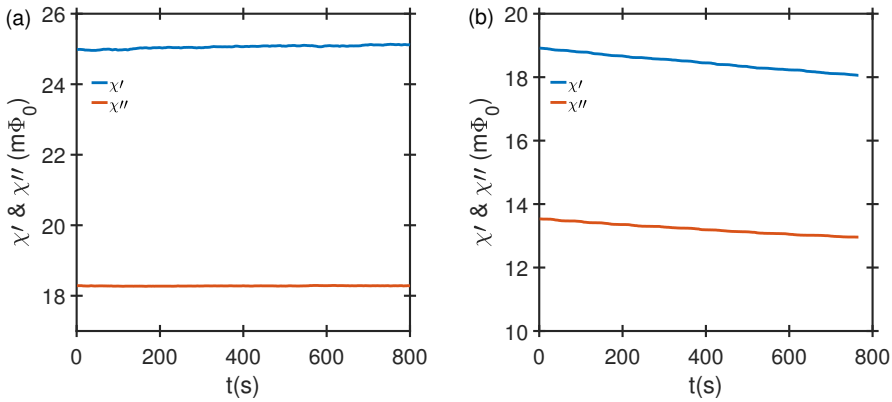

Figure 4.4: The real and imaginary ac susceptibility of (a) uncoated-MNPs (median size of 80 nm) and (b) streptavidin-coated MNPs (median size of 100 nm) measured as a function of time at a constant frequency of 251 Hz and 63 Hz, respectively. The real and imaginary parts of the ac susceptibility show very small change over time for uncoated-MNPs while for streptavidin-coated particles they decrease as a function of time.

process can be observed in two different ways. One in terms of observing a raise at a low frequency with increasing RCA concentration. Since the conjugated MNPs with DNA coils have large hydrodynamic volumes their Brownian relaxation frequency are at very low frequencies, below 1 Hz. The other one is by means of measuring the reduction of the peak amplitude of the imaginary part due to binding of MNPs to large DNA coils.

Samples with various concentrations of RCA coils ranging from 0 to 30 pM (pico-mole/l) were prepared and measured. The real and imaginary components of the magnetic ac susceptibility are measured in the frequency range of 1 to 3000 Hz and are shown in Fig. 4.5(a) and (b), respectively. The negative control (NC) sample contains only functionalized MNPs with mass concentration of 50 µg/ml, and zero concentration (0 pM) of RCA. According to the Cole-Cole formula Eq.(2.10), the imaginary ac susceptibility component for the NC sample reaches a maximum at 60 Hz. This peak frequency (Brownian relaxation frequency) is lower compared with non-functionalized MNPs due to the presence of oligonucleotides on the surface of the MNPs. The functionalization increases the hydrodynamic volume and in turn decreases the Brownian relaxation frequency (from 80 Hz to 60 Hz). Both the real and imaginary ac susceptibility components decrease as the concentration of RCA coils increases, see Fig. 4.5 (a) and (b), respectively.

The amplitude of both the real part at 1 Hz and the imaginary part at 60 Hz continuously decrease with increasing RCA concentration. This decrease is due to a

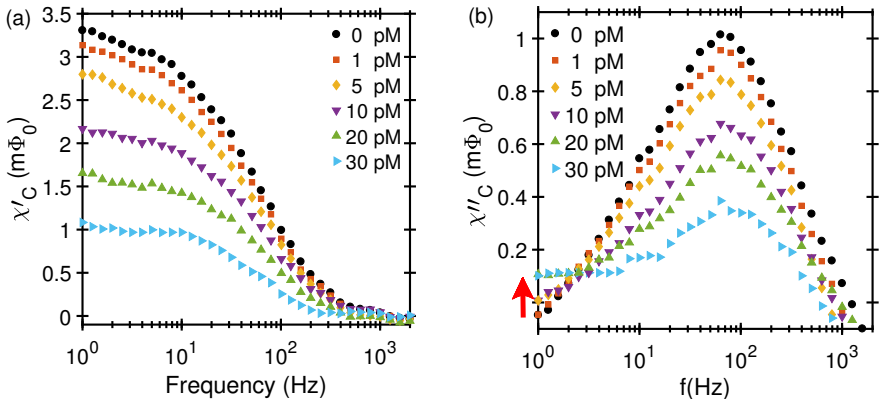

Figure 4.5: (a) Real and (b) imaginary parts of the ac susceptibility as a function of excitation frequency for different concentrations of RCA coils ranging from 0 (negative control NC) to 30 pM in a total volume of 3µL. The drop in the amplitude of both real and imaginary components of the susceptibility indicates the increase in the number of RCA coils and fewer numbers of unbound MNPs in the solution. The red arrow shows a raise in the low frequency tail of the response with increasing RCA concentration.

reduction of the number of free functionalized MNPs in the solution as for increasing RCA concentration the functionalized MNPs are hybridized (and hence immobilized) to the DNA coils. The effective hydrodynamic volume of the MNPs bound to very large DNA coils increases and the Brownian relaxation frequency decreases well below 10 Hz (the Brownian relaxation frequency of the 1 µm RCA coils is in the range of 0.4 Hz). The red arrow in Fig. 4.5 (b) indicates this response. The increase in the imaginary part of the magnetic susceptibility signal below 10 Hz may be due to the appearance of this low frequency peak. The low frequency peak is more pronounced for higher concentrations of RCA coils due to the greater ratio of bound MNPs to free MNPs. It is also worth mentioning that there is a small increase in the frequency of Brownian relaxation for higher RCA concentrations. This may be due to the fact that larger MNPs in the sample distribution precede the smaller ones in hybridizing with RCA coils [3].

The limit of detection for RCA coils is estimated by extracting the amplitudes of the imaginary component of the ac susceptibility at 60 Hz for every RCA concentration. The extinction is a difference between the peak amplitude of the NC sample (0 pM concentration) and the peak amplitudes of the RCA concentrations, $\chi''_{NC} - \chi''_{C}$. Therefore, it determines the number of MNPs that were bound to the RCA coils. Extrapolating the linear dependence of extinction to the noise floor of the sensor corresponds to an estimated LOD of about 1.0×10^5 RCA coils. This limit is

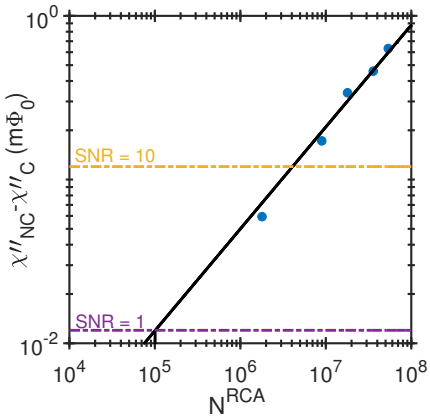

Figure 4.6: The extinction signal ($\chi''_{NC} - \chi''_C$) for different concentrations of the RCA coils at the peak frequency of 60 Hz as a function of number of RCA coils in each corresponding concentration. The linear extrapolation gives a sensitivity of 1.0×10^5 RCA coils in a 3 µL sample volume at SNR = 1.

equivalent to 66 fM of target analyte in the 3 µL sample volume, Fig. 4.6.

4.3.1 Estimation of number of MNPs per DNA coil

The ultimate sensitivity of the bioassay is determined by the iron content sensitivity and by the number of MNPs per single DNA coil. In all samples with RCA coils we had the same concentration of functionalized MNPs (50 µg/mL). Therefore, the extinction of their ac susceptibility signal magnitude compared to the NC (the black dotted line in Fig. 4.5 (a) and (b)) corresponds to the number of functionalized MNPs bound to RCA coils. Using the slope, S, of the linear dependence of the signal to the number of MNPs, Fig. 4.1, the remaining number of unbound functionalized MNPs, N_C^{unbnd}, is estimated and the number of functionalized MNPs bound to RCA coils, N_C^{bnd}, is:

$$\begin{aligned} N_C^{unbnd} &= \frac{\chi''_C}{S}, \\ N_C^{bnd} &= N_{NC} - N_C^{unbnd} \end{aligned} \tag{4.1}$$

where χ''_C is the maximum amplitude of the peak in the imaginary part of the ac susceptibility for a RCA concentration of C and N_{NC} is the number of particles in the NC sample. Dividing the number of bound MNPs by the number of RCA coils for each RCA concentration gives the average number of MNPs per RCA coil, g_{MNP}:

$$g_{MNP} = \frac{N_C^{bnd}}{N_C^{RCA}} = \frac{1}{N_C^{RCA} \times S}(\chi''_{NC} - \chi''_C) \tag{4.2}$$

where χ''_{NC} is the maximum amplitude of the peak in the imaginary part of the ac susceptibility for NC sample and N_C^{RCA} is the number of RCA coils in the sample with RCA coil concentration of C. The estimated g_{MNP} from the lowest to the highest concentration of RCA coils ranges from 3.6 to 1.3 MNPs per coil. We obtain on average 2 MNPs per RCA coil, which is a close estimation to the evaluated mean value of 3 MNP per RCA coil using the DynoMag system [3]. Analysing the RCA coils conjugated with 130 nm MNPs using transmission electron microscopy (TEM) also shows that the average number of MNPs per coil is around 2 [68].

4.4 MNP agglutination experiments

The monomers produced from digesting the RCA coils were used for the identification of the target analyte. The assay is described in Sec. 2.1.6 and we measure the agglutination of MNPs by monomers using magnetic ac susceptibility. Upon the introduction of monomers, the two MNP probes start to agglomerate as they each can only conjugate to one side of the monomer sequence. The agglomeration creates agglutinated clusters of MNPs with large hydrodynamic volume. The change in this hydrodynamic volume is then detected by magnetic ac susceptibility. For this purpose, two identical MNP systems (100 nm in median size) are functionalized with two oligonucleotides which match different regions of the padlock probe. These functionalized MNPs are detection probes and link together in the presence of monomers inducing an agglutination. The clustering of MNPs due to the presence of the monomers is then measured using ac susceptibility. The detection and quantification of the agglutinated probes is determined by measuring the change in the imaginary part of the ac susceptibility. Fig. 4.7 shows the imaginary part of the ac susceptibility as a function of frequency for different monomer concentrations. The NC sample with 0 nM concentration of monomers has equal amounts of solid content from the two MNPs probes with a total solid content concentration of 200 µg/ml. The NC sample is used as a reference. The three samples with monomer concentration of: 23, 46 and 227 nM are also prepared with the same solid content of the two probes. The aggregation of the two probes in the presence of the monomers forms clusters with large hydrodynamic size. Therefore, their response lags behind the external applied field at lower frequencies. In this case, a decrease in the peak amplitude of the imaginary susceptibility and an increase at lower frequency is observed. The decrease in the peak amplitude is due to the clustering of the two MNP probes and the raise at the low frequency is due to the larger hydrodynamic size of the agglutinated clusters.

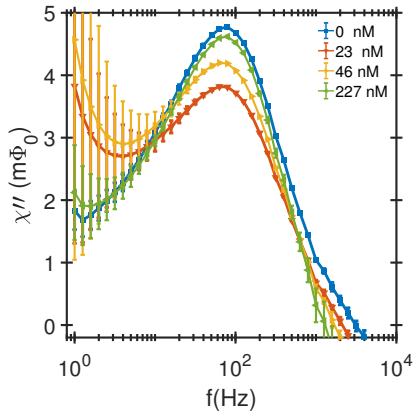

Figure 4.7: Imaginary ac susceptibility as a function of applied excitation field for 0 nM (negative control) and three different concentration of monomers: 23, 46 and 227 nM.

Although by increasing the monomer concentration one would expect to see more agglomeration, the opposite effect is observed. This is because the number of monomers is much larger compared to the number of two probe MNPs that instead of increasing the probability of clustering between the probes they occupy all available sites on the particles making them less likely to agglomerate. For example, in the sample with 227 nM monomer concentration, there are 300 monomers available per single MNP probe, thus, the monomers attach to almost all available sites on both MNP probes making it less likely for the two probes to agglomerate. The large error bars at low frequency (below 10 Hz) is from the MNP clusters formed from agglutination. The large size of the clusters make them colloidally unstable and they immobilize inside the channel. This can be observed dynamically by consequently measuring on the sample which is resting inside the microfluidic channel. Fig. 4.8 shows three consequent measurements of 23 nM monomer concentration in a span of an hour. Below 10 Hz, the amplitude of the imaginary susceptibility drops down over time while the peak amplitude keeps the same amplitude.

4.4.1 Magnetic incubation of monomers

To increase the chance of the two probes meeting and agglutinating in the presence of the monomers, magnetic incubation can be used. A magnetic incubation is done by placing the incubating sample on a magnet. The collection of the suspended MNPs over the magnet increases the chance of the two probes meeting and forming a cluster. The magnet that was used in these experiments is a small block magnet with a surface field of 650 mT. Two different magnetic incubation protocols have

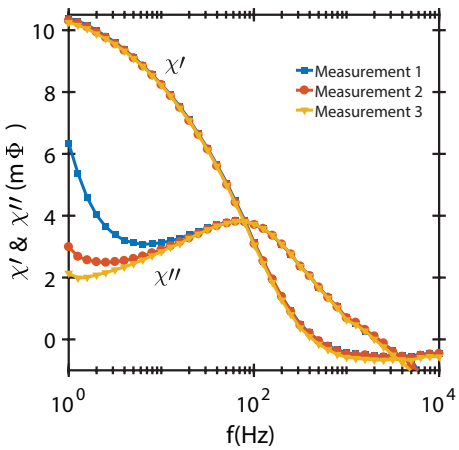

Figure 4.8: Real and imaginary ac susceptibility versus applied magnetic excitation frequency of a sample containing 23 nM monomers, measured 3 times in a row. The sample was pumped inside the microfluidic channel and was not moved during the three measurements. The blue curve is measured right after filling the microfluidic channel followed by the second and third measurements, red and yellow curves respectively. Each measurement takes roughly 20 minutes therefore, the figure shows how the imaginary susceptibility below 10 Hz changes over time.

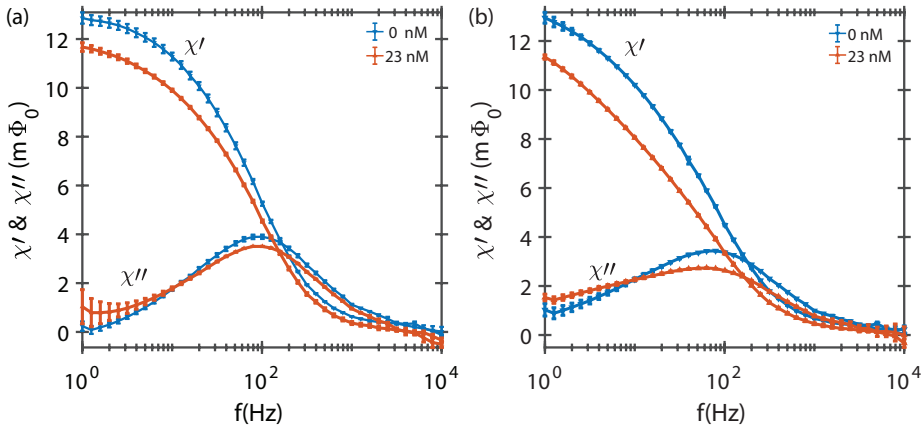

Figure 4.9: (a) The real and imaginary magnetic susceptibility versus excitation field frequency from samples with 0 and 23 nM monomers incubated (a) without any applied field and (b) within external dc field for 30 minutes. There is a slight shift in the peak amplitude frequency of the NC sample due to magnetic incubation, from 100 Hz to 79 Hz.

been used and compared. In the first incubation protocol the sample is incubated in the presence of the magnetic field for 30 minutes. The NC samples are also incubated with the magnet. Fig. 4.9 shows the results from a sample with 23 nM monomer concentration which was (a) incubated without magnet and (b) in the presence of the magnet. The drops in the peak of imaginary susceptibility are 400 and 725 µV for the incubation without and with magnet, respectively.
The second protocol for magnetic incubation does not use the magnet during the whole 30 minutes of incubation. In this protocol, the incubation is carried out without the magnet for the first 28 minutes and then for only 1 minute the sample is placed on a magnet collecting all the suspended MNPs on it. The final minute is given for the re-suspension of the MNPs in the solution. The NC samples also followed the same incubation protocol. The ac susceptibility of samples with 0 and 23 nM monomer concentration is plotted in Fig. 4.10. Using this protocol, no shift in the frequency of the imaginary susceptibility peak amplitude was observed and the drop of the amplitude was around 1261 µV which is 3 times more than the value obtained from the incubation without any magnets. Therefore, applying magnetic field during incubation, improves the hybridization kinetics and significantly increases the signals from the samples. Further studies are required to find the optimal incubation condition to maximize the drop in the peak amplitude of the imaginary susceptibility.

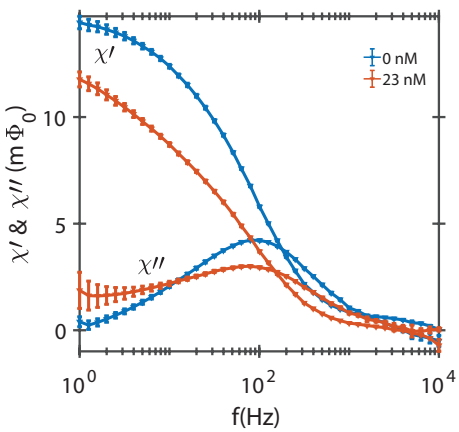

Figure 4.10: Ac magnetic susceptibility measured as a function of frequency for monomer samples with 0 and 23 nM concentration. The samples were incubated inside an applied magnetic field for only 1 minute.

5
Conclusions

A magnetic bioassay based on a high-T_c SQUID gradiometer sensor was demonstrated to have an excellent limit of detection. The DNA assay implements RCA as an amplification technique for the detection of DNA target molecules. The magnetic ac susceptibility measurement was used to detect the specific binding of the MNP markers to the target DNA molecule. An advantage of using the ac susceptibility is very low background signal. The detection signal is the imaginary component of the ac susceptibility and comes only from the MNPs response. The measurements of the liquid suspended MNPs in the microfluidic chip show an ultimate magnetic sensitivity of 2.5 ng and leads to a LOD to DNA target analyte of 0.2×10^{-18} mole. The LOD is comparable to the state-of-the-art ELISA assays [69]. However, our magnetic assay is much faster (2 hours) and does not require multiple washing steps.

The ultra-high sensitivity combined with short turn-around-time is promising for applications in future POC diagnostic system, where all steps of the assay are implemented on a disposable lab-on-a-chip. The assay is not limited to a single target molecule and can be adopted for various DNA and RNA targets. One of the drawbacks, however, is the need for liquid nitrogen to operate our high-T_c SQUID. Recently, we have demonstrated the successful operation and noise measurements of a high-T_c SQUID utilizing a commercial two stage micro electro mechanical system (MEMS) based Joule-Thomson micro-cooler, from Kryoz Technologies BV [2]. The micro-cooler offers long operation time, simple usage, and temperature stability and adjustment. It can also be integrated with the disposable lab-on-a-chip microfluidic sample handler. The magnetic bioassay is therefore very promising for implementation in future POC diagnostic systems.

5.1 Outlook

The biosensing sensitivity of our magnetic bioassay is determined by the sensitivity of the magnetic readout and the number of MNPs conjugated per single RCA coil. Increasing the excitation field amplitude would proportionally increase the magnetic

sensitivity of our ac susceptibility system and consequently the LOD to target analyte. An estimated number of 2 MNPs per coil was calculated for the current assay. However, there are many more sites available for binding of the MNPs. Understanding the kinetics of MNP hybridization with RCA coils could help to improve the number of MNPs per RCA coil. Increasing the number of amplification steps by applying the C2CA protocol would also increase the sensitivity to target analyte. This would, however, increase the total turnaround time of the bioassay.
Although the magnetic bioassay presented here has an excellent performance, it is still far from practical applications. Further work is required on tackling the remaining issues before the assay is ready for practical field applications. Major obstacles include replacing the liquid nitrogen with a closed cycle dry cooler and the full implementation of the assay on a lab-on-a-chip.

Bibliography

[1] S. Sepehri et al. “Volume-amplified magnetic bioassay integrated with microfluidic sample handling and high-Tc SQUID magnetic readout”. *APL Bioengineering* 2.1 (Mar. 2018), p. 016102.

[2] A. Kalabukhov et al. “Operation of a high-Tc SQUID gradiometer with a two-stage MEMS-based Joule Thomson micro-cooler”. *Supercond. Sci. Technol.* 29.9 (2016), p. 095014.

[3] F. Ahrentorp et al. “Sensitive magnetic biodetection using magnetic multi-core nanoparticles and RCA coils”. *J. Magn. Magn. Mater.* (2016), pp. 14–18.

[4] C.-Y. Zhang et al. “Single-quantum-dot-based DNA nanosensor”. *Nat. Mater.* 4 (Oct. 2005), p. 826.

[5] F. Lisdat and D. Schäfer. “The use of electrochemical impedance spectroscopy for biosensing”. *Anal. Bioanal.Chem.* 391.5 (Apr. 2008), p. 1555.

[6] T. Vo-Dinh, F. Yan, and M. B. Wabuyele. “Surface-enhanced Raman scattering for medical diagnostics and biological imaging”. *J. Raman Spectrosc.* 36.6-7 (2005), pp. 640–647.

[7] J.-i. Hahm and C. M. Lieber. “Direct Ultrasensitive Electrical Detection of DNA and DNA Sequence Variations Using Nanowire Nanosensors”. *Nano Lett.* 4.1 (Jan. 2004), pp. 51–54.

[8] W. Wang et al. “Magnetoresistive performance and comparison of supermagnetic nanoparticles on giant magnetoresistive sensor-based detection system”. *Sci. Rep.* 4 (July 2014), p. 5716.

[9] F. W. Østerberg et al. “On-Chip Detection of Rolling Circle Amplified DNA Molecules from Bacillus Globigii Spores and Vibrio Cholerae”. *Small* 10.14 (2014), pp. 2877–2882.

[10] A. P. Astalan et al. “Biomolecular reactions studied using changes in Brownian rotation dynamics of magnetic particles”. *Biosens. Bioelectron.* 19.8 (2004), pp. 945–951.

[11] Y. Du and S. Dong. “Nucleic Acid Biosensors: Recent Advances and Perspectives”. *Anal. Chem.* 89.1 (Jan. 2017), pp. 189–215.

[12] D.-K. Yang et al. “Enhancement of target-DNA hybridization efficiency by pre-hybridization on sequence-orientated micro-arrayed probes”. *J. Chin. Inst. Chem. Eng.* 39.3 (May 2008), pp. 187–193.

[13] K. B. Mullis, F. Ferre, and R. A. Gibbs, eds. *The Polymerase Chain Reaction*. Springer Science+Business Media, LLC, 1994.

[14] T. Notomi et al. “Loop-mediated isothermal amplification of DNA”. *Nucleic Acids Res.* 28.12 (Apr. 2000), e63–e63.

[15] M. Wiedmann et al. “Ligase chain reaction (LCR)–overview and applications.” *Genome Res.* 3.4 (1994), S51–S64.

[16] J. Banér et al. “Signal amplification of padlock probes by rolling circle replication.” *Nucleic Acids Res.* 26.22 (Nov. 1998), pp. 5073–5078.

[17] Q. A. Pankhurst et al. “Applications of magnetic nanoparticles in biomedicine”. *J. Phys. D: Appl. Phys.* 36.13 (2003), R167.

[18] S. Schrittwieser et al. “Homogeneous Biosensing Based on Magnetic Particle Labels”. *Sensors* 16.6 (2016), p. 828.

[19] J. Kudr et al. “Magnetic Nanoparticles: From Design and Synthesis to Real World Applications”. *Nanomaterials* 7.9 (2017).

[20] A.-H. Lu, E. L. Salabas, and F. Schüth. “Magnetic Nanoparticles: Synthesis, Protection, Functionalization, and Application”. *Angew. Chem. Int. Ed.* 46.8 (2007), pp. 1222–1244.

[21] H. C. Tekin and M. A. M. Gijs. “Ultrasensitive protein detection: a case for microfluidic magnetic bead-based assays”. *Lab. Chip* 13.24 (2013), pp. 4711–4739.

[22] A. Sandhu. “Biosensing: New probes offer much faster results”. *Nat Nano* 2.12 (Dec. 2007), pp. 746–748.

[23] Y. Zhao et al. “Isothermal Amplification of Nucleic Acids”. *Chem. Rev.* 115.22 (Nov. 2015), pp. 12491–12545.

[24] V. Gubala et al. “Point of Care Diagnostics: Status and Future”. *Anal. Chem.* 84.2 (Jan. 2012), pp. 487–515.

[25] M. Fakruddin et al. “Nucleic acid amplification: Alternative methods of polymerase chain reaction”. *Journal of Pharmacy & Bioallied Sciences* 5.4 (Aug. 2013), pp. 245–252.

[26] M. Nilsson et al. “Padlock probes: circularizing oligonucleotides for localized DNA detection”. *Science* 265.5181 (1994), pp. 2085–2088.

[27] D.-O. Antson et al. “PCR-generated padlock probes detect single nucleotide variation in genomic DNA”. eng. *Nucleic Acids Res.* 28 (12 June 2000), e58.

[28] T. Zardán Gómez de la Torre. “Detection of Biomolecules Using Volume-Amplified Magnetic Nanobeads”. PhD thesis. Uppsala University, Department of Engineering Sciences, Nanotechnology and Functional Materials., 2012.

[29] R. Jansson. “Development of a solid-phase padlock probe technology using microfluidics”. MA thesis. Uppsala University School of Engineering, Aug. 2007.

[30] T. Zardán Gómez de la Torre et al. “Detection of rolling circle amplified DNA molecules using probe-tagged magnetic nanobeads in a portable AC susceptometer”. *Biosens. Bioelectron.* 29.1 (2011), pp. 195–199.

[31] M. Kühnemund et al. “Sensitive and inexpensive digital DNA analysis by microfluidic enrichment of rolling circle amplified single-molecules”. *Nucleic Acids Res.* 45.8 (2017), e59.

[32] F. Dahl et al. “Circle-to-circle amplification for precise and sensitive DNA analysis”. *Proc. Natl. Acad. Sci. U.S.A.* 101.13 (2004), pp. 4548–4553.

[33] A. Mezger et al. “Scalable DNA-Based Magnetic Nanoparticle Agglutination Assay for Bacterial Detection in Patient Samples”. *ACS Nano* 9.7 (2015), pp. 7374–7382.

[34] J. B. Haun et al. “Magnetic nanoparticle biosensors”. *Wiley Interdiscip. Rev. Nanomed. Nanobiotechnol.* 2.3 (2010), pp. 291–304.

[35] A. V. Bychkova et al. “Multifunctional biocompatible coatings on magnetic nanoparticles”. *Russ. Chem. Rev.* 81.11 (2012), p. 1026.

[36] J. Dieckhoff et al. “Magnetic-field dependence of Brownian and Néel relaxation times”. *J. Appl. Phys.* 119.4 (2016), p. 043903.

[37] M. I. Shliomis. “Magnetic fluids”. *Soviet Physics Uspekhi* 17.2 (1974), p. 153.

[38] B. K. P. Scaife. “On the low-field, low-frequency susceptibility of magnetic fluids”. *J. Phys. D: Appl. Phys.* 19.10 (1986), p. L195.

[39] P. J. W. Debye. *Polar molecules*. New York, The Chemical Catalog Company, 1929.

[40] P. C. Fannin, S. W. Charles, and T. Relihan. “On the influence of inertial effects, arising from rotational Brownian motion, on the complex susceptibility of ferrofluids”. *J. Phys. D: Appl. Phys.* 28.9 (1995), p. 1765.

[41] J. Connolly and T. G. S. Pierre. “Proposed biosensors based on time-dependent properties of magnetic fluids”. *J. Magn. Magn. Mater.* 225.1-2 (2001). Proceedings of the Third International Conference on Scientific and Clinical Applications of Magnetic Carriers, pp. 156–160.

[42] A. Prieto Astalan et al. “Magnetic response of thermally blocked magnetic nanoparticles in a pulsed magnetic field”. *J. Magn. Magn. Mater.* 311.1 (Apr. 2007), pp. 166–170.

[43] V. L. Calero-DdelC, D. I. Santiago-Quinonez, and C. Rinaldi. “Quantitative nanoscale viscosity measurements using magnetic nanoparticles and SQUID AC susceptibility measurements”. *Soft Matter* 7 (2011), pp. 4497–4503.

[44] P. C. Fannin, B. K. P. Scaife, and S. W. Charles. “The measurement of the frequency dependent susceptibility of magnetic colloids”. *J. Magn. Magn. Mater.* 72.1 (Mar. 1988), pp. 95–108.

[45] K. S. Cole and R. H. Cole. “Dispersion and Absorption in Dielectrics I. Alternating Current Characteristics”. *The Journal of Chemical Physics* 9.4 (Apr. 1941), pp. 341–351.

[46] A. Fornara et al. “Tailored Magnetic Nanoparticles for Direct and Sensitive Detection of Biomolecules in Biological Samples”. *Nano Lett.* 8.10 (Oct. 2008), pp. 3423–3428.

[47] K. Enpuku et al. “Biosensing utilizing magnetic markers and superconducting quantum interference devices”. *Supercond. Sci. Technol.* 30.5 (2017), p. 053002.

[48] S. Y. Yang et al. “Clinic Applications in Assaying Ultra-Low-Concentration Bio-Markers Using HTS SQUID-Based AC Magnetosusceptometer”. *IEEE Trans. Appl. Supercond.* 23 (2013), p. 1600604.

[49] M. Donolato et al. “Novel Readout Method for Molecular Diagnostic Assays Based on Optical Measurements of Magnetic Nanobead Dynamics”. *Anal. Chem.* 87.3 (2015), pp. 1622–1629.

[50] M. Donolato et al. “Quantification of rolling circle amplified DNA using magnetic nanobeads and a Blu-ray optical pick-up unit”. *Biosens. Bioelectron.* 67 (2015), pp. 649–655.

[51] F. Öisjöen et al. “Fast and Sensitive Measurement of Specific Antigen-Antibody Binding Reactions With Magnetic Nanoparticles and HTS SQUID”. *IEEE Trans. Appl. Supercond.* 19.3 (June 2009), pp. 848–852.

[52] F. Öisjöen et al. “A new approach for bioassays based on frequency- and time-domain measurements of magnetic nanoparticles”. *Biosens. Bioelectron.* 25.5 (2010), pp. 1008–1013.

[53] J. J. Chieh et al. “Hyper-high-sensitivity wash-free magnetoreduction assay on biomolecules using high-Tc superconducting quantum interference devices”. *J. Appl. Phys.* 103.1 (Jan. 2008), p. 014703.

[54] M. Strömberg et al. “Sensitive Molecular Diagnostics Using Volume-Amplified Magnetic Nanobeads”. *Nano Lett.* 8.3 (2008), pp. 816–821.

[55] F. Ahrentorp et al. “Effective particle magnetic moment of multi-core particles”. *J. Magn. Magn. Mater.* 380 (2015), pp. 221–226.

[56] M. K. Wu et al. “Superconductivity at 93 K in a new mixed-phase Y-Ba-Cu-O compound system at ambient pressure”. *Phys. Rev. Lett.* 58 (9 Mar. 1987), pp. 908–910.

[57] J. Clarke and A. I. Braginski, eds. *The SQUID Handbook: Fundamentals and Technology of SQUIDs and SQUID Systems, Volume I.* Wiley-VCH Verlag GmbH & Co. KGaA, Weinheim, FRG, 2004.

[58] T. V. Duzer and C. W. Turner. *Principles of Superconductive Devices and Circuits, 2nd Edition.* Prentice Hall, 1999.

[59] F. Öisjöen. “High-Tc SQUIDs for biomedical applications: immunoassays, MEG and ULF-MRI”. PhD thesis. Department of Microtechnology and Nanoscience - MC2, Chalmers University of Technology., 2011.

[60] F. Öisjöen et al. “High-Tc SQUID gradiometer system for immunoassays”. *Supercond. Sci. Technol.* 21.3 (2008), p. 034004.

[61] T. M. Squires and S. R. Quake. “Microfluidics: Fluid physics at the nanoliter scale”. *Rev. Mod. Phys.* 77 (3 Oct. 2005), pp. 977–1026.

[62] E. K. Sackmann, A. L. Fulton, and D. J. Beebe. "The present and future role of microfluidics in biomedical research". *Nature* 507 (Mar. 2014), p. 181.

[63] A. Dietzel, ed. *Microsystems for Pharmatechnology*. Springer International Publishing, 2016. ISBN: 978-3-319-26920-7.

[64] H. Becker and C. Gärtner. "Polymer microfabrication technologies for microfluidic systems". *Anal. Bioanal.Chem.* 390.1 (Jan. 2008), pp. 89–111.

[65] J. C. McDonald et al. "Fabrication of microfluidic systems in poly (dimethylsiloxane)". *Electrophoresis* 21.1 (2000), pp. 27–40.

[66] D. Kim and A. E. Herr. "Protein immobilization techniques for microfluidic assays". *Biomicrofluidics* 7.4 (July 2013), p. 041501.

[67] H. Zhang and M. Chiao. "Anti-fouling Coatings of Poly(dimethylsiloxane) Devices for Biological and Biomedical Applications". *Journal of Medical and Biological Engineering* 35.2 (Apr. 2015), pp. 143–155.

[68] S. Akhtar et al. "Real-Space Transmission Electron Microscopy Investigations of Attachment of Functionalized Magnetic Nanoparticles to DNA-Coils Acting as a Biosensor". *The Journal of Physical Chemistry B* 114.41 (2010), pp. 13255–13262.

[69] R. Wilson. "Sensitivity and specificity: twin goals of proteomics assays. Can they be combined?" *Expert Rev. Proteomics* 10.2 (2013), pp. 135–149.